Bachelor's thesis
The Bachelor's Programme in Physical Sciences
Theoretical Physics

# Theoretical Investigations of Superconducting Qubits Under a Subharmonic Drive

Nikolai Argatoff

September 15, 2024

Supervisor: Professor Mikko Möttönen

Advisors: PhD Vasilii Vadimov
MSc Aashish Sah

Examiner: PhD Esko Keski-Vakkuri

University of Helsinki
Faculty of Science

PL 64 (Gustaf Hällströmin katu 2a)
00014 Helsingin yliopisto

HELSINGIN YLIOPISTO — HELSINGFORS UNIVERSITET — UNIVERSITY OF HELSINKI

| Tiedekunta — Fakultet — Faculty | Koulutusohjelma — Utbildningsprogram — Degree programme |
|---|---|
| Faculty of Science | The Bachelor's Programme in Physical Sciences<br>Theoretical Physics |

Tekijä — Författare — Author

Nikolai Argatoff

Työn nimi — Arbetets titel — Title

Theoretical Investigations of Superconducting Qubits Under a Subharmonic Drive

| Työn laji — Arbetets art — Level | Aika — Datum — Month and year | Sivumäärä — Sidantal — Number of pages |
|---|---|---|
| Bachelor's thesis | September 15, 2024 | 50 |

Tiivistelmä — Referat — Abstract

Achieving quantum speedup on intermediate-scale quantum processors requires the implementation of high-fidelity gate operations. Quantum gates are typically executed using electromagnetic driving fields tuned to the resonance frequency of the qubit; however, this resonant drive degrades qubit coherence and leads to the loss of quantum information. A recently proposed control method, subharmonic driving, involves driving the qubit at one-third of its resonant frequency. This technique enables decoupling from the resonant decay channel, allowing it to be filtered out.

In this thesis, we analytically investigate the decoherence of a transmon qubit under voltage fluctuations caused by subharmonic driving. We use harmonic analysis techniques commonly used in non-equilibrium statistical mechanics to investigate the effects of a noisy subharmonic Hamiltonian. Our results show that the average infidelity scales inversely with the mean photon number in the infinite photon limit, matching the scaling observed with resonant driving.

While subharmonic driving is not found to improve infidelity scaling, we identify a potential new discovery: vacuum noise at five-thirds of the qubit frequency contributes to the decay rate through a multiphoton process.

Avainsanat — Nyckelord — Keywords

Superconducting qubits, subharmonic driving, quantum noise, Langevin equation, spectral density

Säilytyspaikka — Förvaringsställe — Where deposited

Muita tietoja — Övriga uppgifter — Additional information

# Preface

I would like to thank my thesis supervisor, Professor Mikko Möttönen, for his encouragement, insightful advice and the opportunity to explore new ideas in the quantum world at QCD. I also express my gratitude to my thesis advisors, PhD candidate Aashish Sah and PhD Vasilii Vadimov for their guidance, limitless patience under the borbardment of questions and kindness. I thank PhD Paolo Muratore Ginanneschi for illuminating discussions. I am grateful to PhD Esko Keski-Vakkuri for kindly agreeing to formally examine this thesis.

Nikolai Argatoff
15.9.2024

# Contents

# 1. Introduction

The promise of harnessing quantum phenomena to solve classically intractable problems has driven rapidly increasing investment in the field of quantum computing [1]. Even though several quantum algorithms have theoretically demonstrated quantum speedup [2, 3], the achievement of practical quantum advantage requires noise-tolerant hardware. An crucial aspect of this effort is creating qubits with long coherence times, enabling them to perform complex computations effectively.

Among the various qubit technologies [4], superconducting qubits stand out as a promising candidate [5]. Fabricated on a chip, superconducting qubits offer scalability and therefore meet the first of DiVincenzo's criteria for constructing a quantum computer [6]. Additionally, superconducting circuits benefit from modern manufacturing processes, which allows for configurability and precise design. However, the information inside a superconducting qubit is short-lived with typical coherence times around $100\mu$s and state-of-the-art implementations reaching up to millisecond coherence [7].

To overcome this challenge, superconducting qubits require manipulation through fast operating schemes. Their states can be precisely controlled using microwave pulses that propagate through transmission lines to coupling ports. Traditionally, the frequency of the control field is tuned to match the transition frequency between the qubit's ground and excited states, enabling efficient qubit excitation and rapid gate operations. While resonant driving is a standard method for executing qubit gates, it exhibits an inherent contradiction between achieving fast operations and maintaining long coherence times.

To protect a quantum bit from uncontrollable perturbations, it must be isolated from the environment. Yet, external interactions are unavoidable because qubit state preparation, control, and measurement inevitably expose the qubit to environmental influences [8]. Achieving faster gate operations requires stronger coupling to the drive line, but this also increases the qubit's exposure to noisy fluctuations within the transmission line. On the other hand, weaker coupling leads to longer gate times, which can be compensated by increasing the drive strength. However, higher applied power causes the circuitry to heat up, degrading coherence. This unavoidable trade-off is a consequence of choosing to control the qubit at its natural transition frequency.

Recently, it has shown that the transmon qubit can be driven at one-third of its tran-

sition frequency, enabling high-speed gate operations [9]. The charge-insensitive transmon is the most widely adopted among the various superconducting qubit families [10]. Thanks to its intrinsic non-linearity, this subharmonic drive produces a Rabi rate proportional to the cube of the applied voltage, in contrast to the linear relationship in the resonant case. Beyond the scaling advantages of the cubic power law, subharmonic driving enables filtering of the transition frequency from the drive, providing enhanced protection against resonant decay [9].

Even though quantum circuits are operated at millikelvin temperatures where thermal fluctuations are reduced, the drive line is occupied by the zero-point energy flucutations [11]. As the quantum noise is an irreducible part of qubit control, theoretical understanding of decoherence sources is required to improve the fidelity of quantum gates.

In this thesis we aim to study theoretically the behaviour of the noisy subharmonic drive. Our main objective is to investigate whether the subharmonic drive provides more favourable gate fidelities compared to the resonant driving. In [12], this goal was examined within a simulation framework, allowing us to compare the results of simulations with our mathematical calculations.

In Chapter 2, we present a thorough discussion of the foundations of superconducting circuits, the transmon qubit, and quantum driving at resonance. Chapter 3 introduces the preliminaries of classical and quantum noise along with the tools of harmonic analysis for investigating fluctuating systems subject to random forces. In Chapter 4, we integrate the frameworks of superconducting qubits and non-equilibrium systems to investigate the noisy subharmonic drive. This chapter provides a detailed discussion of the subharmonic drive, derives the corresponding noisy subharmonic Hamiltonian, and presents comprehensive computations of the qubit decay rate. Lastly, Chapter 5 provides a summary of our findings and concluding remarks.

# 2. Theory of Quantum circuits

A qubit is mathematically represented as a linear combination of basis states in a two-dimensional Hilbert space. These orthogonal states are denoted as $|0\rangle$ and $|1\rangle$, analogous to the truth values in Boolean algebra. Unlike a classical bit, a quantum bit can exist in a superposition of states:

$$|\psi\rangle = \alpha|0\rangle + \beta|1\rangle, \tag{2.1}$$

where the complex numbers $\alpha$ and $\beta$ satisfy the normalization condition $|\alpha|^2 + |\beta|^2 = 1$. To implement a physical qubit, any quantum system whose dynamics can be confined to just two states is, in principle, suitable.

In this chapter, we present how a qubit can be realized using superconducting circuit elements. As with many reviews in the field [5, 13, 14], we begin with a simple LC resonant circuit and demonstrate that non-linearity is essential for qubit formation. By introducing a non-linear component called the Josephson junction, we then examine charge and transmon qubits, and briefly discuss their control mechanisms.

## 2.1 Quantization of an LC circuit

To better understand the quantum mechanical theory of electric circuits, we begin with preliminaries in classical circuit analysis. As shown in Fig. 2.1, an LC circuit consists of an inductor and a capacitor connected in parallel, with inductance $L$ and capacitance $C$ respectively.

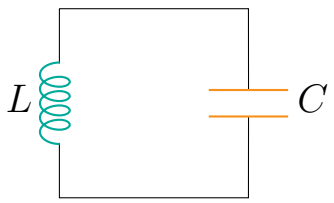


**Figure 2.1:** A circuit diagram of an LC resonator.

The standard approach to solve the behaviour of the circuit begins with the constitutive relations

$$\Phi = LI, \quad \text{and} \quad V_C = \frac{Q}{C}, \tag{2.2}$$

where $\Phi$ is the magnetic flux across the inductor, $I$ is current, $V_C$ is voltage and $Q$ is the charge across the capacitor. If $V$ is the voltage drop between the terminals of an inductor, then flux and voltage are related by Faraday's Law

$$\Phi(t) = \int_{-\infty}^{t} \mathrm{d}\tau\, V(\tau), \tag{2.3}$$

where we assume that far in the past the voltage is zero. Combined with charge conservation $Q(t) = \int_{-\infty}^{t} \mathrm{d}\tau I(\tau)$, we may rewrite the equations above in the differential form

$$V = L\frac{\mathrm{d}I}{\mathrm{d}t}, \quad \text{and} \quad -\frac{\mathrm{d}V}{\mathrm{d}t} = \frac{I}{C}, \tag{2.4}$$

where we also substituted $V_C = -V$. By decoupling these two differential equations, we obtain the equation of a linear harmonic oscillator

$$\frac{\mathrm{d}^2V}{\mathrm{d}t^2} = -\omega_r^2 V. \tag{2.5}$$

where $\omega_r = 1/\sqrt{LC}$ is the resonant angular frequency. The voltage across the inductor oscillates sinusoidally at angular frequency $\omega_r$ as energy is transferred between the inductor's magnetic field and the capacitor's electric field.

An alternative way to obtain the dynamical equations of an LC circuit is the Hamiltonian formulation. The procedure for deriving a Hamiltonian of a general circuit is well-established in literature [11]. Here, we identify the Hamiltonian of the LC circuit as the total energy

$$H_{\mathrm{LC}} \coloneqq \frac{1}{2}CV^2 + \frac{1}{2}LI^2. \tag{2.6}$$

For quantum circuits it is conventional to give the role of the position coordinate to the generalized flux $\Phi$ defined in Eq. (2.2) with charge $Q$ becoming canonically conjugate momentum. With this choice, the Hamiltonian is of the form

$$H_{\mathrm{LC}} = \frac{Q^2}{2C} + \frac{1}{2}C\omega_r^2\Phi^2, \tag{2.7}$$

where the angular frequency $\omega_r$ highlights the analogy with the mechanical oscillator. To quantize the circuit, we promote the charge and flux coordinates to quantum operators satisfying canonical commutation relation

$$[\hat{\Phi}, \hat{Q}] = \mathrm{i}\hbar. \tag{2.8}$$

The quantum counterpart of Eq. (2.7) is the Hamiltonian of the quantum harmonic oscillator (QHO). Using the textbook approach we introduce bosonic annihilation $\hat{a}^\dagger$ and creation $\hat{a}$ operators [15]

$$\hat{\Phi} = \sqrt{\frac{\hbar}{2\omega_r C}}(\hat{a}^\dagger + \hat{a}), \quad \hat{Q} = \mathrm{i}\sqrt{\frac{\hbar\omega_r C}{2}}(\hat{a}^\dagger - \hat{a}), \tag{2.9}$$

which obey the commutation relation $[\hat{a}, \hat{a}^\dagger] = 1$. The Hamiltonian transforms to

$$\hat{H}_{\mathrm{LC}} = \hbar\omega_r \left(\hat{a}^\dagger\hat{a} + \frac{1}{2}\right), \tag{2.10}$$

where the product $\hat{n} = \hat{a}^\dagger\hat{a}$ is called the number operator. With some algebraic manipulations, the eigenstates of the number operator can be shown to be Fock states $|n\rangle$, where $n$ is an integer number of excitations. The operator $\hat{a}$ lowers the excitation by one number, while the creation operator $\hat{a}^\dagger$ raises it by one number:

$$\hat{a}^\dagger\hat{a}|n\rangle = n|n\rangle, \quad \hat{a}|n\rangle = \sqrt{n}|n-1\rangle, \quad \hat{a}^\dagger|n\rangle = \sqrt{n+1}|n+1\rangle, \quad n \in \mathbb{N}, \tag{2.11}$$

giving the operators their respective names. The energy spectrum of the Hamiltonian is therefore found to be

$$E_n = \hbar\omega_r \left(n + \frac{1}{2}\right), \tag{2.12}$$

where $E_n$ is the energy of $n$-th eigenstate. As can be seen from Fig. 2.2a, the energy levels of quantum LC circuit are equidistantly spaced which is problematic for the construction of a functioning qubit. Efforts to control the two lowest energy states also excite higher energy levels due to the linearity of our circuit elements.

## 2.2 Josephson junction

A Josephson junction is a non-linear superconducting circuit element that was theoretically predicted by Josephson [16]. The junction is formed by two superconducting leads separated by a thin insulating barrier as illustrated in Fig. 2.3. The insulator is thin enough for quantum tunneling of Cooper pairs to occur between the superconductors.

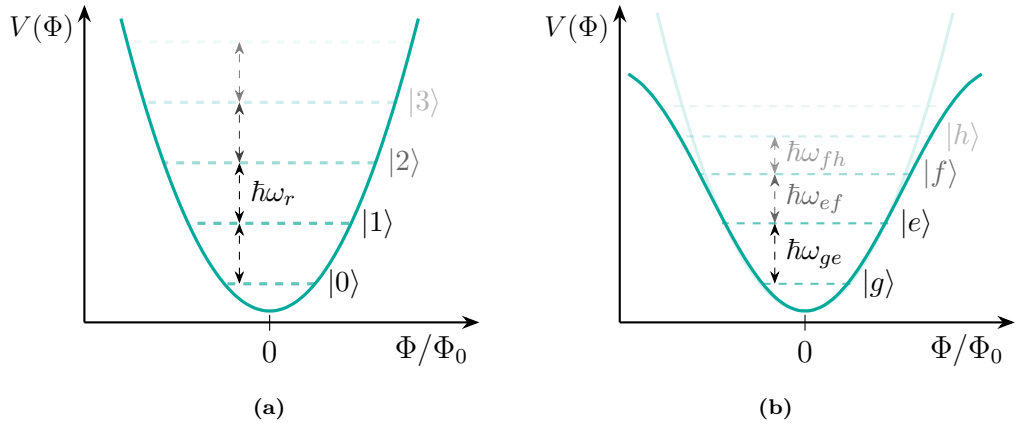


**Figure 2.2:** Schematic illustrations of (a) the harmonic potential of the LC circuit with equidistant energy levels of. (b) the cosine potential of the Cooper-pair box. The energy states labeled by $\{|g\rangle, |e\rangle, |f\rangle, \ldots\}$ are non-equidistant.

The resulting current $I$ passes the junction with zero voltage drop and is given by the expression

$$I(t) = I_c \sin\left(\varphi(t)\right), \tag{2.13}$$

where $\varphi(t)$ is the phase difference of the many-particle condensate wavefunction across the junction and the critical current $I_c$ is a constant of the fabricated component [17]. As predicted by London [18], the magnetic flux through a superconducting loop takes only integer values

$$\Phi = n\Phi_0, \quad n \in \mathbb{N}, \tag{2.14}$$

where the magnetic flux quantum was experimentally verified to be $\Phi_0 = h/2e$ with $2e$ being the Cooper pair charge.

Applying a voltage difference across the junction $V$ increases the phase difference with time as follows [17]:

$$\dot{\varphi}(t) = \frac{2\pi}{\Phi_0} V(t). \tag{2.15}$$

Integrating both sides of Eq. (2.15), we obtain

$$\varphi(t) = \frac{2\pi}{\Phi_0} \int_{-\infty}^{t} \mathrm{d}\tau V(\tau) = \frac{2\pi}{\Phi_0} \Phi(t), \tag{2.16}$$

where the above result is taken modulo $2\pi$ as the phase difference is a periodic quantity. Therefore, by combining the two Josephson's relations Eq. (2.13) and Eq. (2.15), we obtain

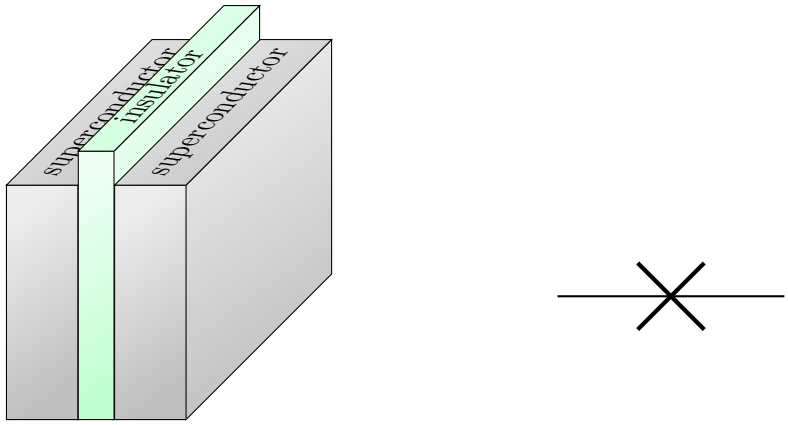


(a) (b)

**Figure 2.3:** The Josephson junction: (a) Schematic diagram, (b) Electrical symbol.

$$I = I_c \sin\left(\frac{2\pi}{\Phi_0}\Phi(t)\right), \tag{2.17}$$

which when inverted gives

$$\Phi(t) = \frac{\Phi_0}{2\pi} \sin^{-1}\left(\frac{I}{I_c}\right). \tag{2.18}$$

This relationship between the flux and the current bears resemblance to the case of linear inductance $\Phi = LI$, where $L$ is independent of flux. The Josephson's junction is therefore akin to a non-linear inductor, with inductance

$$L(\Phi) = \frac{\mathrm{d}\Phi}{\mathrm{d}I} = \frac{\Phi_0}{2\pi I_c} \frac{1}{\cos\left(2\pi\Phi/\Phi_0\right)}. \tag{2.19}$$

The inductive energy $E_L$ of an idealized junction with zero capacitance is expressed as follows:

$$\begin{aligned} E_L &= \int_{-\infty}^{t} \mathrm{d}\tau V(\tau) I(\tau) \\ &= \int_{-\infty}^{t} \mathrm{d}\tau \dot{\Phi}(\tau) I_c \sin\left(\frac{2\pi}{\Phi_0}\Phi(\tau)\right) \\ &= E_\mathrm{J}\left[1 - \cos\left(\frac{2\pi}{\Phi_0}\Phi(\tau)\right)\right], \end{aligned} \tag{2.20}$$

where we defined a constant $E_\mathrm{J} = \Phi_0 I_c/2\pi$ referred to as the Josephson energy. In reality, the charge accumulation at the ends of the leads gives rise to some self-capacitance $C_\mathrm{J}$. The resulting capacitive energy is taken pictorially into account by shunting the junction by a dummy capacitor as Fig. 2.4 demonstrates.

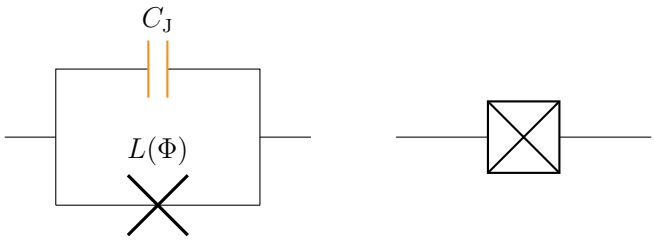


**Figure 2.4:** The self-capacitance $C_J$ of the junction can be modeled by a capacitor connected in parallel to the idealized junction (left). This configuration is represented by drawing the cross with the box (right).

## 2.3 The Cooper-pair box

The Cooper-pair box (CPB) [19], shown in Fig. 2.5a, consists of a Josephson junction connected to a voltage source $V$ via a gate capacitance $C_g$. The region between the junction and the gate capacitance is called a superconducting island to which Cooper pairs are transferred from the reservoir. The quantization of the CPB Hamiltonian yields

$$\hat{H} = \frac{(\hat{Q} - Q_g)^2}{2C_\Sigma} - E_J \cos\left(\frac{2\pi}{\Phi_0}\hat{\Phi}\right), \tag{2.21}$$

where $C_\Sigma = C_g + C_J$ is the total capacitance [13]. The offset charge $Q_g$ arises from an applied voltage bias or environmental fluctuations. Using the Eq. (2.16) we introduce the phase operator $\hat{\varphi}$ and proceed to adopt a number-phase representation where the Hamiltonian takes the form

$$\hat{H} = 4E_C(\hat{n} - n_g)^2 - E_J \cos\hat{\varphi}, \tag{2.22}$$

where we defined the charge number operator $\hat{n} = \hat{Q}/2e$ which represents the number of excess Cooper pairs on the island. We also introduced the charging energy $E_C = e^2/(2C_\Sigma)$ and an offset $n_g = Q_g/(2e)$.

Due to the influence of the cosine potential, the energy levels of the CPB Hamiltonian are no longer evenly spaced, as illustrated in Fig. 2.2b. The eigenstates can be described using the Mathieu functions and are typically denoted as $\{|g\rangle, |e\rangle, |f\rangle, \ldots\}$. For simplicity, we will continue to use the labels $\{|0\rangle, |1\rangle, |2\rangle, \ldots\}$, with the understanding that these states no longer correspond to the Fock states of the QHO. The anharmonicity of the system enables the CPB to function as a qubit, allowing us to isolate the two lowest energy levels for computation. [13]

To be more precise, the circuit Fig. 2.5a is called the CPB when the charging energy dominates with $E_C \geq E_J$. The initial superconducting circuit studies favoured this

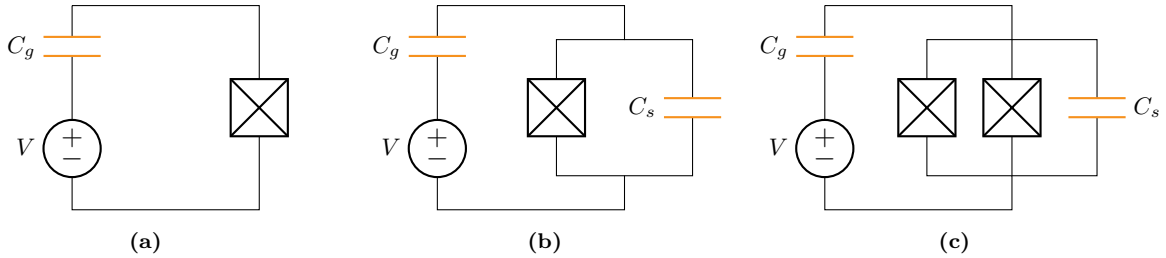


**Figure 2.5:** Circuit diagram of (a) the Cooper-pair box (b) the transmon qubit (c) the flux-tunable transmon qubit

capacitive regime as a large $E_C/E_\mathrm{J}$ ratio provides high anharmonicity. However, the transition frequency is then modulated by the change in the offset $n_g$ which makes the CPB highly susceptible to charge noise. Therefore it is suitable to consider what happens in the opposite case $E_\mathrm{J} \geq E_C$.

## 2.4 The transmon qubit

The transmon is currently one of the most widely used qubit designs [10]. It was shown that increasing $E_\mathrm{J}/E_C$ decreases the relative anharmonicity as a weak power law, the charge dispersion decreases *exponentially*. Therefore, for large $E_\mathrm{J}/E_C$ the charge noise sensitivity can be greatly supressed while still retaining enough anharmonicity necessary for a functioning qubit.

Fig. 2.5b shows the basis for the transmon where the CPB is shunted with large capacitance $C_s$ decreasing the charging energy $E_C$. Since the Josephson junction and the shunt capacitor are connected in parallel, the Hamiltonian of the transmon is inherited from Eq. (2.22) with a substitution $C_\mathrm{J} \to C_\mathrm{J}+C_s$. In contrast to the CPB, the fluctuations of the phase $\hat{\varphi}$ are small in the transmon regime, allowing us to expand the cosine to [10]

$$\hat{H} = 4E_C\hat{n}^2 + \frac{1}{2}E_\mathrm{J}\hat{\varphi}^2 - \frac{1}{12}E_\mathrm{J}\hat{\varphi}^4 - E_\mathrm{J}, \tag{2.23}$$

where we have dropped charge offset $n_g$ since its influence is suppressed on the lowest energy levels. We note that the first two terms in Eq. (2.23) give the linear dynamics of the QHO while the fourth order term $\hat{\varphi}^4$ provides the necessary non-linearity. Therefore, analogous to Eq. (2.9), we are prompted to again introduce the creation $\hat{q}^\dagger$ and annihilation $\hat{q}$ operators [10]

$$\hat{\varphi} = \left(\frac{2E_C}{E_\mathrm{J}}\right)^{1/4}(\hat{q}^\dagger + \hat{q}), \quad \hat{n} = \frac{\mathrm{i}}{2}\left(\frac{E_\mathrm{J}}{2E_C}\right)^{1/4}(\hat{q}^\dagger - \hat{q}). \tag{2.24}$$

With these definitions, we obtain

$$\hat{H} = \hbar\omega_p \hat{q}^\dagger \hat{q} - \frac{E_C}{12}(\hat{q}^\dagger + \hat{q})^4 - E_\mathrm{J}. \tag{2.25}$$

where we defined $\omega_p = \sqrt{8E_C E_\mathrm{J}}/\hbar$ known as the Josephson plasma frequency. Treating Eq. (2.25) as a QHO with a quartic perturbation term, the unperturbed energies are seen to be

$$\mathrm{e}_n^{(0)} = -E_\mathrm{J}\sqrt{8E_C E_\mathrm{J}}(n + \frac{1}{2}), \tag{2.26}$$

which is analogous to Eq. (2.12) up to a constant. Using time-independent perturbation theory, the first order corrections are found to be given by

$$\mathrm{e}_n^{(1)} = -\frac{E_C}{12}\langle n|(\hat{q}^\dagger + \hat{q})^4|n\rangle = -\frac{E_C}{12}(6n^2 + 6n + 3). \tag{2.27}$$

Calculating the energy difference between transitions $e$-$g$ and $e$-$f$, we get

$$\begin{aligned} E_{0\to1} &\coloneqq E_1 - E_0 = \sqrt{8E_C E_\mathrm{J}} - E_C \\ E_{1\to2} &\coloneqq E_2 - E_1 = \sqrt{8E_C E_\mathrm{J}} - 2E_C. \end{aligned} \tag{2.28}$$

It follows that the absolute and relative anharmonicities between transitions are

$$E_{1\to2} - E_{0\to1} = -E_C, \quad \frac{E_{1\to2} - E_{0\to1}}{E_{0\to1}} = \left(\frac{8E_\mathrm{J}}{E_C}\right)^{-1/2}, \tag{2.29}$$

which coincides with the claim of $E_\mathrm{J}/E_C$ scaling at the beginning of this section. The anharmonicity $-E_C$ is large enough to restrict the dynamics of the transmon to the two lowest energy levels, leading us to define the transmon qubit frequency $\omega_q$ in the form of

$$\omega_q \coloneqq \frac{E_{0\to1}}{\hbar} = \frac{\sqrt{8E_C E_\mathrm{J}} - E_C}{\hbar} = \omega_p + \alpha, \tag{2.30}$$

where we defined the anharmonicity (of the angular frequencies) $\alpha = -E_C/\hbar$ and made use of the Josephson plasma frequency $\omega_p$ in the transmon Hamiltonian Eq. (2.25).

For the qubit frequency $\omega_q$ to arise explicitly in the Hamiltonian we need to expand the product in Eq. (2.25). Upon doing so it is customary to perform the rotating-wave approximation (RWA) in which only the terms with an equal number of $\hat{q}^\dagger$ and $\hat{q}$ are kept. One motivation for the RWA is seen from the frame rotating at $\omega_q$, where the terms oscillate if the number of operators $\hat{q}^\dagger$ and $\hat{q}$ in it is unequal. If the prefactor of such terms

is much smaller than the frequency of oscillation they average out. Performing RWA for Eq. (2.25), we obtain

$$\hat{H}_{\mathrm{T}}^{\mathrm{RWA}} \approx \hbar\omega_q \hat{q}^\dagger \hat{q} + \frac{\alpha}{2}\hat{q}^\dagger \hat{q}^\dagger \hat{q}\hat{q}, \tag{2.31}$$

where wrote the Hamiltonian in terms of $\omega_q$ and $\alpha$ defined in Eq. (2.30). This form of the transmon Hamiltonian is commonly used in literature, but in some situations the RWA hides important dynamics as in the case of subharmonic driving.

## 2.5 Tunable coupling and dc SQUID

Once the circuit elements of the transmon have been fabricated, the qubit frequency $\omega_q$ is fixed according to Eq. (2.30). To construct more refined quantum computer architectures one would like the transmon frequency to be a tunable parameter.

One popular modification to the transmon, that results in a tunable transmon frequency, is to replace the Josephson junction with a loop of two junctions connected in parallel. Such a loop is called a dc superconducting quantum interference device (dc-SQUID) and, invented already in 1964 [20], is vastly used in applications as a highly sensitive magnetometer. Making the replacement, the transmon Hamiltonian becomes

$$\hat{H}_{\mathrm{T}} = 4E_C(\hat{n} - n_g)^2 - E_{J1}\cos\hat{\varphi}_1 - E_{J2}\cos\hat{\varphi}_2, \tag{2.32}$$

where the Josephson energy and the phase difference of junction $i$ are $E_{Ji}$ and $\hat{\varphi}_i$ respectively [13]. Applying an external flux $\Phi_{\mathrm{ext}}$ and ignoring the inductance of electrodes themselves, with the flux quantization condition Eq. (2.14) we have

$$\hat{\varphi}_1 - \hat{\varphi}_2 = \frac{2\pi\Phi_{\mathrm{ext}}}{\Phi_0}, \tag{2.33}$$

which is again expressed as modulo $2\pi$. By defining an average phase difference $\hat{\varphi} = (\hat{\varphi}_1 - \hat{\varphi}_2)/2$, we get

$$\hat{\varphi}_1 = \hat{\varphi} + \frac{\pi\Phi_{\mathrm{ext}}}{\Phi_0}, \quad \hat{\varphi}_2 = \hat{\varphi} - \frac{\pi\Phi_{\mathrm{ext}}}{\Phi_0}. \tag{2.34}$$

Now, the inductive terms in the Hamiltonian Eq. (2.32) can be expanded to

$$\begin{aligned} E_{\mathrm{J1}}\cos\hat{\varphi}_1 + E_{\mathrm{J2}}\cos\hat{\varphi}_2 &= (E_{J2} + E_{J1})\cos\left(\frac{\pi\Phi_{\mathrm{ext}}}{\Phi_0}\right)\cos\hat{\varphi} + (E_{\mathrm{J2}} - E_{\mathrm{J1}})\sin\left(\frac{\pi\Phi_{\mathrm{ext}}}{\Phi_0}\right)\sin\hat{\varphi} \\ &= E_{\mathrm{J}\Sigma}\cos\left(\frac{\pi\Phi_{\mathrm{ext}}}{\Phi_0}\right)\left[\cos\hat{\varphi} + d\tan\left(\frac{\pi\Phi_{\mathrm{ext}}}{\Phi_0}\right)\sin\hat{\varphi}\right], \end{aligned} \tag{2.35}$$

where we have defined the combined energy $E_{\mathrm{J}\Sigma} = E_{\mathrm{J}1} + E_{\mathrm{J}2}$ and the junction asymmetry $d = (E_{\mathrm{J}2} - E_{\mathrm{J}1})/E_{\mathrm{J}\Sigma}$. Defining the phase $\tan\varphi_0 = d\tan(\pi\Phi_{\mathrm{ext}}/\Phi_0)$ and using a simple trigonometric addition identity* Eq. (2.35) can be written as

$$E_{\mathrm{J}\Sigma}\cos\left(\frac{\pi\Phi_{\mathrm{ext}}}{\Phi_0}\right)\sqrt{1+d^2\tan^2\left(\frac{\pi\Phi_{\mathrm{ext}}}{\Phi_0}\right)}\cos(\hat{\varphi}-\varphi_0). \tag{2.36}$$

Therefore the Hamiltonian Eq. (2.32) can be written as

$$\hat{H}_{\mathrm{T}} = 4E_C(\hat{n}-n_g)^2 - E_{\mathrm{J}}(\Phi_{\mathrm{ext}})\cos(\hat{\varphi}-\varphi_0), \tag{2.37}$$

with the effective flux dependent Josephson energy

$$E_{\mathrm{J}}(\Phi_{\mathrm{ext}}) = E_{\mathrm{J}\Sigma}\cos\left(\frac{\pi\Phi_{\mathrm{ext}}}{\Phi_0}\right)\sqrt{1+d^2\tan^2\left(\frac{\pi\Phi_{\mathrm{ext}}}{\Phi_0}\right)}. \tag{2.38}$$

For time-independent flux, the phase $\varphi_0$ can be eliminated with a change of variables. Thus comparing Eq. (2.32) and Eq. (2.37), we conclude that replacing the single junction with a dc-SQUID gives remarkably the same transmon Hamiltonian but with a flux-tunable transmon frequency.

$$\omega_q(\Phi_{\mathrm{ext}}) = \frac{\sqrt{8E_CE_{\mathrm{J}}(\Phi_{\mathrm{ext}})}-E_C}{\hbar}, \tag{2.39}$$

which can be now adjusted to a desired value by modifying the external flux.

## 2.6 Transmission lines

It goes without saying that for the superconducting circuits to be useful, we need the means of interaction to manipulate and read out their state, and to couple them to each other. Qubit control can be realized with quantized electromagnetic fields confined in the coplanar waveguide resonator (CPW) [13]. Compared to the LC oscillator with a single microwave tone, the coplanar wavequide functions as a transmission line that propagates a continuum of frequencies. The transmission line is a *distributed* element and it is equivalent to an array of inductive and capacitive lumped elements as shown in Fig. 2.6. Therefore, the standard circuit quantization technique can be utilized to derive the transmission line Hamiltonian:

*$A\cos\alpha + B\sin\alpha = \sqrt{A^2+B^2}(\frac{A}{\sqrt{A^2+B^2}}\cos\alpha + \frac{B}{\sqrt{A^2+B^2}}\sin\alpha) = \cos(\alpha-\beta)$, where $\beta = \tan(B/A)$

$$\hat{H}_{\text{tml}} = \sum_{n=0}^{\infty} \hbar\omega_n \hat{b}_n^\dagger \hat{b}_n, \tag{2.40}$$

where each mode operator $\hat{b}_n$ and mode frequency $\omega_n$ are determined by the boundary conditions and transmission line parameters [13]. The interaction between a transmon and the transmission line is modeled by constructing the interaction Hamiltonian using the transmon ladder operators $\hat{q}$ and the mode operators $\hat{b}_n$. Taking into account only one resonator mode leads to extensively studied Jaynes-Cummings interaction [21]. In this thesis, we use a semi-classical model where the transmission line fields are treated classically.

However, understanding the quantized modes is essential for analyzing dissipation. While the transmission line enables control of the qubit state, it also couples the qubit to uncontrollable degrees of freedom causing decoherence, as discussed in Section 3.4.

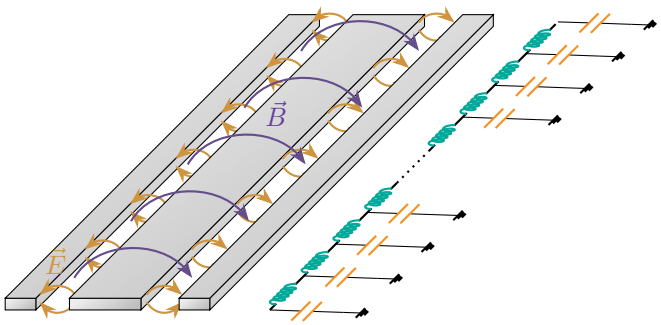


**Figure 2.6:** A schematic diagram of the coplanar waveguide resonator (left) and its corresponding circuit model (right). The center conductor is positioned between two ground planes, with electric and magnetic fields indicated.

## 2.7 Qubit drive

To showcase how the single qubit control can be realized, we couple the transmon capacitively to a semi-infinite transmission line*. Here, we consider the drive as a coherent classical field of frequency $\omega_d$ and phase $\varphi_d$ with the Hamiltonian that reads [14]

$$\hat{H} = \hat{H}_{\text{T}}^{\text{RWA}} + \hat{H}_{\text{d}}(t), \tag{2.41}$$

where $\hat{H}_T^{\text{RWA}}$ is the transmon Hamiltonian in Eq. (2.31) and the driving Hamiltonian $\hat{H}_d(t)$ reads

*For the detailed derivation of the electric-dipole interaction between the transmission line and the qubit see [13].

$$\hat{H}_d(t) = \mathrm{i}\hbar\Omega\cos(\omega_d t + \varphi_d)(\hat{q}^\dagger - \hat{q}). \tag{2.42}$$

Above the operator $i(\hat{q}^\dagger - \hat{q})$ is proportional to the voltage operator (see Eqs. (2.2) and (2.9)) and angular frequency $\Omega$ is the strength of the drive. After truncating to the computational subspace, Eq. (2.41) reads

$$\hat{H} = -\frac{\hbar\omega_q}{2}\hat{\sigma}_z + \hbar\Omega\cos(\omega_d t + \varphi_d)\hat{\sigma}_y. \tag{2.43}$$

Next, with the unitary transformation $\hat{U}_\mathrm{R} = \mathrm{e}^{-\mathrm{i}\omega_q t\sigma_z/2}$, we transition to the rotating frame using the following identity

$$\hat{U}_\mathrm{R}\hat{\sigma}_y\hat{U}_\mathrm{R}^\dagger = \cos(\omega_q t)\hat{\sigma}_y - \sin(\omega_q t)\hat{\sigma}_x. \tag{2.44}$$

The transformed Hamiltonian reads

$$\begin{aligned}
\hat{H}_\mathrm{R} &= \hat{U}_\mathrm{R}\hat{H}\hat{U}_\mathrm{R}^\dagger + \mathrm{i}\dot{\hat{U}}_\mathrm{R}\hat{U}_\mathrm{R}^\dagger \\
&= \hbar\Omega\cos(\omega_d t + \varphi_d)\left[\cos(\omega_q t)\hat{\sigma}_y - \sin(\omega_q t)\hat{\sigma}_x\right] \\
&= \frac{\hbar\Omega}{4}\Big[\left(\mathrm{e}^{\mathrm{i}(\omega_q-\omega_d)t-\mathrm{i}\varphi_d} + \mathrm{e}^{\mathrm{i}(\omega_q+\omega_d)t+\mathrm{i}\varphi_d} + \mathrm{e}^{-\mathrm{i}(\omega_q+\omega_d)t-\mathrm{i}\varphi_d} + \mathrm{e}^{-\mathrm{i}(\omega_q-\omega_d)t+\mathrm{i}\varphi_d}\right)\hat{\sigma}_y \\
&\quad + \mathrm{i}\left(\mathrm{e}^{\mathrm{i}(\omega_q-\omega_d)t-\mathrm{i}\varphi_d} + \mathrm{e}^{\mathrm{i}(\omega_q+\omega_d)t+\mathrm{i}\varphi_d} - \mathrm{e}^{-\mathrm{i}(\omega_q+\omega_d)t-\mathrm{i}\varphi_d} - \mathrm{e}^{-\mathrm{i}(\omega_q-\omega_d)t+\mathrm{i}\varphi_d}\right)\hat{\sigma}_x\Big].
\end{aligned} \tag{2.45}$$

By invoking the rotating wave approximation (RWA), we drop the fast-rotating terms (those with $\omega_q + \omega_d$), simplifying the Hamiltonian to:

$$\begin{aligned}
\hat{H}_\mathrm{R}^\mathrm{RWA}(\delta t, \varphi_d) &= \frac{\hbar\Omega}{4}\Big[\left(\mathrm{e}^{\mathrm{i}(\delta t-\varphi_d)} + \mathrm{e}^{-\mathrm{i}(\delta t-\varphi_d)}\right)\hat{\sigma}_y + \mathrm{i}\left(\mathrm{e}^{\mathrm{i}(\delta t-\varphi_d)} - \mathrm{e}^{-\mathrm{i}(\delta t-\varphi_d)}\right)\hat{\sigma}_x\Big] \\
&= \frac{\hbar\Omega}{2}\Big[\cos[\delta t - \varphi_d]\hat{\sigma}_y - \sin[\delta t - \varphi_d]\hat{\sigma}_x\Big]
\end{aligned} \tag{2.46}$$

with $\delta = \omega_q - \omega_d$ the detuning between the qubit and the drive angular frequencies. For resonant drive $\delta = 0$, the choice of $\varphi_d = 0$ leads to rotations about the $y$-axis

$$\hat{H}_\mathrm{R}^\mathrm{RWA}(0, 0) = \frac{\hbar\Omega}{2}\hat{\sigma}_y \tag{2.47}$$

and the choice of $\varphi_d = \pi/2$ leads to rotations about the $x$-axis

$$\hat{H}_\mathrm{R}^\mathrm{RWA}\left(0, \frac{\pi}{2}\right) = \frac{\hbar\Omega}{2}\hat{\sigma}_x. \tag{2.48}$$

To explicitly perform a pulse around $x$-axis, we set $\varphi_d = \pi/2$ and obtain the propagator

$$\hat{U}_x(t) = \mathrm{e}^{-\mathrm{i}\Omega t\hat{\sigma}_x/2} = \cos\left[\frac{\Omega}{2}t\right]\hat{I} - \mathrm{i}\sin\left[\frac{\Omega}{2}t\right]\hat{\sigma_x}, \tag{2.49}$$

where $\hat{I}$ is the identity operator. The state function $|\psi(t)\rangle$ under the evolution of the rotating frame Hamiltonian can now be written as

$$|\psi(t)\rangle = \hat{U}_x(t)|0\rangle, \tag{2.50}$$

where we have chosen the qubit initially to be in the ground state $|\psi(0)\rangle = |0\rangle$. It's easy to see that a pulse duration of $t = \pi/\Omega$ flips the qubit to the excited state:

$$\hat{U}_x(t = \frac{\pi}{\Omega})|0\rangle = -\hat{\sigma}_x|0\rangle = -|1\rangle, \tag{2.51}$$

where the minus sign is a non-measurable global phase. Note, that this evolution is described in the rotating frame. The probability of measuring the qubit in the excited state as a function of time $t$ takes the form

$$P_e(t) = \left|\langle 1|\hat{U}_x(t)|0\rangle\right|^2 = \sin^2\left[\frac{\Omega}{2}t\right]. \tag{2.52}$$

From the above equation, we see that applying a resonant drive causes qubit to oscillate between the ground and excited state. These oscillations, called Rabi oscillations, also arise in the general case of Eq. (2.46), where the Hamiltonian can be rewritten as:

$$\hat{H}_{\mathrm{R}}^{\mathrm{RWA}}(\delta t, \varphi_d) = \mathrm{i}\frac{\hbar\Omega}{2}\begin{pmatrix} 0 & -\mathrm{e}^{-\mathrm{i}(\delta t-\varphi_d)} \\ \mathrm{e}^{\mathrm{i}(\delta t-\varphi_d)} & 0 \end{pmatrix}. \tag{2.53}$$

With some further work in solving the Schrödinger equation [22], the probability $P_e(t)$ takes the form

$$P_e(t) = \frac{\Omega^2}{\Omega_{\mathrm{R}}^2}\sin\left(\frac{\Omega_{\mathrm{R}}t}{2}\right), \text{ where } \Omega_{\mathrm{R}} = \sqrt{\delta^2 + \Omega^2}. \tag{2.54}$$

From the above equation, we observe that the probability of finding the qubit in the excited state oscillates at an angular frequency, $\Omega_{\mathrm{R}}$, known as the Rabi rate. Although the Rabi rate increases with larger detuning $\delta$, the amplitude of these oscillations decreases as illustrated in Fig. 2.7. Since the maximum amplitude is achieved at resonance $\delta = 0$, resonant driving is the preferred method for qubit control.

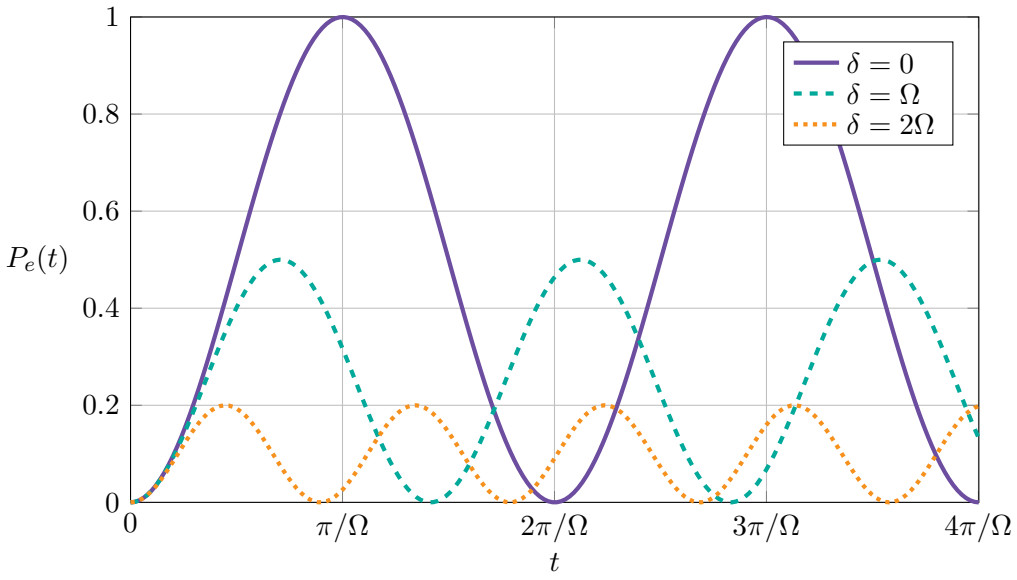


**Figure 2.7:** Rabi oscillations as a function of time for three different detunings $\delta$

# 3. Preliminaries of noisy systems

The effect of uncontrollable fluctuations in a physical system can be studied with the powerful tools of statistical mechanics. In the first half of this chapter, we introduce the basic mathematical concepts of classical random signals following [23, 24, 25]. We demonstrate how harmonic analysis tools can be applied to investigate the statistical properties of classical noise. Then, we establish the Wiener-Khintchine theorem, which describes the duality between a signal's autocorrelation function and its power spectral density. We apply these concepts to derive the spectral density of a Brownian particle following the Langevin equation. Next, we discuss the quantum noise resulting from voltage fluctuations in transmission lines. Finally, we introduce measures to quantify decoherence in qubit operations.

## 3.1 Classical noise

A fluctuating quantity, such as noisy voltage, can be modeled as a series of random variables $V_1, V_2, V_3, \ldots$ where each increment in the index corresponds to a progression in time. Considering time as a continuous parameter, this time series is represented by a random process $V(t)$. Observing $V(t)$ provides a specific realization of the process, giving us a sample function $v(t)$. [23]

The average value of $V$ at time $t$, called the ensemble average, is denoted by the angled brackets

$$\langle V(t)\rangle \coloneqq \int_{-\infty}^{\infty} \mathrm{d}v\, vp(v,t), \tag{3.1}$$

where $p(v,t)$ is some probability distribution. For the *centered* process the average vanishes $\langle V(t)\rangle = 0$. An important quantity of the process $V(t)$ is the *autocorrelation function* $\kappa(t_1,t_2)$ defined by

$$\kappa(t_1,t_2) \coloneqq \langle V(t_1)V(t_2)\rangle. \tag{3.2}$$

Above we implicitly assumed that $V(t)$ is a real random process. For a complex process $Z(t)$ one would define the complex autocorrelation function

$$\kappa(t_1, t_2) \coloneqq \langle Z(t_1)Z^*(t_2)\rangle. \tag{3.3}$$

We consider specifically *stationary* random process meaning that it's statistical properties are invariant under time translation. This has two important consequences i) the ensemble average of the process is constant and ii) the autocorrelation function depends only on the time difference $\tau = t_2 - t_1$, giving

$$\kappa(t_1, t_2) = \kappa(\tau, 0). \tag{3.4}$$

For physical systems it is often assumed that after some finite characteristic *correlation time* $\tau_c$ the autocorrelation function decays rapidly to zero. [23]

From this point forward, we may assume without loss of generality that the stationary process $V(t)$ is centered, i.e., $\langle V(t)\rangle = 0$, due to renormalization.

## 3.2 Harmonic analysis of stationary processes

Significant insights can be obtained by studying the spectral properties of stationary processes. However, working meaningfully with the Fourier series of a process $V(t)$, or even its realization $v(t)$, requires considerable caution. For brevity, we will discuss the spectral decomposition of the process informally. The procedures behind our primarily symbolic descriptions can be found in [23, 25].

We consider a stationary stochastic process $V(t)$ over a time interval $-T/2 < t < T/2$ *. The process $V(t)$ may be symbolically expanded into a Fourier series as

$$V(t) = \sum_{n=-\infty}^{\infty} A_n \mathrm{e}^{-\mathrm{i}\omega_n t}, \tag{3.5}$$

where $\omega_n = 2\pi n/T$ are the angular frequencies and $A_n$ is a random variable defined by

$$A_n = \frac{1}{T}\int_{-T/2}^{T/2} \mathrm{d}t\, V(t)\mathrm{e}^{\mathrm{i}\omega_n t}. \tag{3.6}$$

The stationarity assumption implies

*Due to the assumption of stationarity the location of the interval is arbitrary

$$\begin{aligned}\langle A_n\rangle &= 0, \quad n \neq 0,\\ \langle A_0\rangle &= \langle V\rangle,\end{aligned} \tag{3.7}$$

where the last equality may also be set to zero invoking renormalization. We obtain a second important consequence by expanding the (complex) correlation function

$$\begin{aligned}\kappa(\tau) &= \langle V(t)V^*(t+\tau)\rangle\\ &= \sum_{n=-\infty}^{\infty}\sum_{k=-\infty}^{\infty}\langle A_nA_k^*\rangle \mathrm{e}^{-\mathrm{i}(\omega_n-\omega_k)t}\mathrm{e}^{-\mathrm{i}\omega_n\tau}.\end{aligned} \tag{3.8}$$

As the RHS above should be independent of $t$, we have

$$\langle A_nA_k^*\rangle = \langle |A_n|^2\rangle\delta(n-k), \tag{3.9}$$

where $\delta$ is the Kronecker delta function

$$\delta(n-k) = \begin{cases}1, & \text{if } n=k,\\ 0, & \text{otherwise.}\end{cases} \tag{3.10}$$

Eq. (3.9) implies that the Fourier coefficients of different angular frequencies are uncorrelated, and the autocorrelation function is given by

$$\kappa(\tau) = \sum_{n=-\infty}^{\infty}\langle |A_n|^2\rangle \mathrm{e}^{-\mathrm{i}\omega_n\tau}. \tag{3.11}$$

The above form is hinting at the important relationship we have been building towards. If we first define

$$V[\omega_n] \coloneqq \int_{-T/2}^{T/2}\mathrm{d}t\, V(t)\mathrm{e}^{\mathrm{i}\omega_n t} = TA_n, \tag{3.12}$$

we observe that when taking the limit $T\to\infty$, Eq. (3.12) yields a Fourier transform $V[\omega]$. For finite $T$, the relation Eq. (3.9) may be rewritten as

$$\langle V[\omega_n]V^*[\omega_k]\rangle = \frac{2\pi}{T}\langle |V[\omega_n]|^2\rangle\delta(\omega_n-\omega_k). \tag{3.13}$$

Defining the *power spectral density* $S_{VV}(\omega)$ of the process $V(t)$ as

$$S_{VV}(\omega) = \lim_{T\to\infty} \frac{1}{T}\langle |V[\omega]|^2\rangle, \tag{3.14}$$

we have that in limit $T \to \infty$ Eq. (3.13) reads

$$\langle V[\omega]V^*[\omega']\rangle = 2\pi S_{VV}(\omega)\delta(\omega - \omega'), \tag{3.15}$$

where $\delta$ is now a Dirac's delta function. Coming back to the correlation function in Eq. (3.11), the equivalent limit converts the sum into an integral

$$\kappa(\tau) = \lim_{T\to\infty} \frac{1}{2\pi T}\int_{-\infty}^{\infty} \mathrm{d}\omega \langle |V[\omega]|^2\rangle \mathrm{e}^{-\mathrm{i}\omega\tau}. \tag{3.16}$$

Invoking the definition of the power spectral density in Eq. (3.14), we finally arrive at

$$\kappa(\tau) = \int_{-\infty}^{\infty} \frac{\mathrm{d}\omega}{2\pi} S_{VV}(\omega)\mathrm{e}^{-\mathrm{i}\omega\tau}. \tag{3.17}$$

This result is known as the *Wiener-Khintchine theorem*. It states that the autocorrelation function and the spectral density form a Fourier-transform pair. The reciprocal of Eq. (3.17) gives the inverse transform

$$S_{VV}(\omega) = \int_{-\infty}^{\infty} \mathrm{d}\tau\, \kappa(\tau)\mathrm{e}^{\mathrm{i}\omega\tau}. \tag{3.18}$$

In physical terms, the power spectral density quantifies the noise intensity at a given angular frequency $\omega$. *White noise* represents an extreme case where the power spectral density remains constant:

$$S_{VV}(\omega) = S. \tag{3.19}$$

According to the Wiener-Khintchine theorem, the autocorrelation function of a white noise signal is Dirac's delta function $S\delta(\tau)$, indicating complete lack of correlation across all time intervals. Noise exhibiting a non-constant power spectrum is often termed *colored* and as such has a finite correlation time $\tau_c$.

## 3.3 Langevin equation

Our exposition of harmonic analysis tools is particularly fruitful for solving linear random equations. The behavior of a heavy particle in a fluid subjected to erratic collisions

can be mathematically modeled within the framework of the Langevin equation [24]. The Langevin equation describes the dynamics of nonequilibrium systems subject to a random force. For example, considering the displacement of a Brownian particle in a harmonic potential, Langevin equation reads

$$\ddot{X} + \gamma\dot{X} + \omega_0^2 X = \frac{1}{m}F(t), \tag{3.20}$$

where $X$ is the displacement, $\omega_0$ is the resonant frequency and $\gamma$ is the damping coefficient of a deterministic viscous force. The random force $F(t)$, assumed to be stationary, represents the effect of collisions with other molecules. As this force drives the particle, the displacement $X(t)$ itself becomes a stationary random process. To analyze the statistical behavior of $X(t)$, we substitute the Fourier series representations from Eq. (3.5) into the Langevin equation, leading to the following relation:

$$X_n = \frac{1}{m}\frac{F_n}{\omega_0^2 - \omega_n^2 - \mathrm{i}\omega_n\gamma}, \tag{3.21}$$

where the indexed variables denote the respective Fourier coefficients as defined by Eq. (3.6). Taking the Fourier transform limit, we obtain

$$\begin{aligned} S_{XX}(\omega) &= \frac{1}{m^2}\frac{S_{FF}(\omega)}{|\omega_0^2 - \omega^2 - \mathrm{i}\omega\gamma|^2} \\ &= \frac{1}{m^2}\frac{S_{FF}(\omega)}{(\omega_0^2 - \omega^2)^2 + \omega^2\gamma^2}, \end{aligned} \tag{3.22}$$

which establishes the relation between the spectrum density of the random force $S_{FF}$ and the spectrum density of position $S_{XX}$. The correlation function of the random harmonic oscillator can be then computed using the Wiener-Khintchine theorem

$$\kappa_{XX}(\tau) = \frac{1}{m^2}\int_{-\infty}^{\infty}\frac{\mathrm{d}\omega}{2\pi}\frac{S_{FF}(\omega)}{(\omega_0^2 - \omega^2)^2 + \omega^2\gamma^2}\mathrm{e}^{-\mathrm{i}\omega\tau}. \tag{3.23}$$

If we consider the simplest case of white noise, where the spectrum of $F(t)$ is constant $S_{FF}(\omega) = S_{FF}$, the integrand can be evaluated easily with residue calculus. Assuming $\tau > 0$ we need to close the contour in lower half plane with a semicircle enclosing the two poles

$$\omega = \pm\omega' - i\frac{\gamma}{2}, \quad \text{where } \omega' = \sqrt{\omega_0^2 - \frac{\gamma^2}{4}}. \tag{3.24}$$

Applying Cauchy's residue theorem, the correlation function reads as

$$\kappa_{FF}(\tau) = \frac{S_{FF}}{2m^2\gamma\omega_0^2}\left(\cos(\omega' t) + \frac{\gamma}{2\omega'}\sin(\omega' t)\right)\mathrm{e}^{-\gamma t/2}. \tag{3.25}$$

If we postulate $S_{FF} = 2m\gamma k_{\mathrm{B}}T$ and take $\tau = 0$, we recover the classical equipartition law [24]

$$\kappa_{FF}(0) = \langle X(0)^2\rangle = \frac{k_{\mathrm{B}}T}{m\omega_0^2}. \tag{3.26}$$

We will apply the above procedure to investigate the noisy subharmonic drive in Section 4.2.

## 3.4 Quantum noise in the transmission line

In classical systems, where $V(t)$ is generally a real valued process, the spectral density is symmetric in frequency $S_{VV}[\omega] = S_{VV}[-\omega]$, like in Eq. (4.27). However, in quantum mechanics where classical variables are replaced with operators this is not the case. If we replace a noisy classical signal $V(t)$ by a self-adjoint operator $\hat{V}(t)$, we may define a quantum noise spectral density in analogy with the classical case [8]

$$S_{VV}(\omega) \coloneqq \int_{-\infty}^{\infty} \mathrm{d}\tau\, \langle \hat{V}(\tau)\hat{V}(0)\rangle \mathrm{e}^{\mathrm{i}\omega\tau}. \tag{3.27}$$

As $\hat{V}(t)$ does not have to commute with itself at a different time $t' \neq t$, this leads to frequency asymmetry and zero-point fluctuations. For this reason the quantum noise persists even at absolute zero temperature. To compare, the classical spectral density of voltage noise in a resistor $R$ follows the Johnson-Nyquist formula:

$$S_{VV}(\omega) = 2Rk_{\mathrm{B}}T, \tag{3.28}$$

where the power spectrum becomes negligible at low temperatures $T$. Nyquist showed that the problem of characterizing thermal fluctuations can be circumvented by counting the normal modes of a transmission line connected to it [26]. Each mode contributes an average energy $k_{\mathrm{B}}T$, with Boltzmann's constant $k_B$, reflecting the application of the classical equipartition law.

Transmission lines occupy an even more central role in quantum dissipation modeling. Using the Caldeira-Legget model a physical resistor can be represented by an infinite set of LC oscillators wired in parallel [27]. Despite consisting solely of lossless elements, the infinite length of the line introduces irreversible dynamics: energy injected into the

line propagates as waves to infinity. However, as the Hamiltonian of the circuit is still conservative, the transmission line modes can be quantized. In contrast to Eq. (2.40), when the transmission line is considered to be of infinite length, the frequency spectrum of the modes becomes continuous. For the thorough review, see [11, 8]. The fluctuations of the voltage operator at the end of the transmission line give rise to the power spectral density that reads

$$S_{VV}(\omega) = \frac{2Z_c\hbar\omega}{1 - \mathrm{e}^{-\hbar\omega/k_\mathrm{B}T}}. \tag{3.29}$$

where $Z_c$ is the characteristic impedance of the line. As promised, the *quantum Nyquist spectral density* is asymmetric in frequency. The spectral density at positive frequencies indicates the noisy resistor's capacity to *absorb* energy, while negative frequencies correspond to energy *emission*. It is instructive to define symmetric and anti-symmetric parts of the spectrum

$$S^{+}_{VV}(\omega) = \frac{S_{VV}(\omega) + S_{VV}(-\omega)}{2} = Z_c\hbar\omega\coth(\frac{\hbar\omega}{2k_\mathrm{B}T}) \tag{3.30}$$

$$S^{-}_{VV}(\omega) = \frac{S_{VV}(\omega) - S_{VV}(-\omega)}{2} = Z_c\hbar\omega, \tag{3.31}$$

and to rewrite Eq. (3.29) as

$$S_{VV}(\omega) = S^{+}_{VV}(\omega) + S^{-}_{VV}(\omega) = Z_c\hbar\omega\left(\coth(\frac{\hbar\omega}{2k_\mathrm{B}T}) + 1\right). \tag{3.32}$$

The spectrum $S^{+}_{VV}(\omega)$ is usually taken to represent the total thermal and quantum noise, whereas $S^{-}_{VV}(\omega)$ is linked to dissipation [28]. For high-temperature limit, we obtain the classical Johnson-Nyquist spectrum in Eq. (3.28). In the opposite quantum regime, Eq. (3.29) becomes

$$S_{VV}(\omega) = 2Z_c\hbar\omega\Theta(\omega), \tag{3.33}$$

where the Heaviside's step function $\Theta$ indicates that at absolute zero temperature the resistor can only absorb energy.

## 3.5 Decoherence and fidelity

When a qubit couples with its environment, information about its superposition state is gradually lost. Consequently, qubit control and measurement inevitably lead to decoherence due to the various noise sources involved in the interaction.

The impact of noise on a qubit depends on its coupling axis. With transverse coupling, the interaction is mediated through the off-diagonal elements of the coupling Hamiltonian, leading to energy transfer. This causes qubit excitation $|0\rangle \to |1\rangle$ at a rate $\Gamma_{1\uparrow}$ and decay $|1\rangle \to |0\rangle$ at a rate $\Gamma_{1\downarrow}$. *Transverse noise* is thus responsible for *longitudinal relaxation*, which occurs at the longitudinal relaxation rate $\Gamma_1$, defined as [14]

$$\Gamma_1 \coloneqq \Gamma_{1\uparrow} + \Gamma_{1\downarrow}. \tag{3.34}$$

At low temperatures, the environment is unlikely to excite the qubit, making $\Gamma_{1\uparrow}$ negligible. In contrast, *longitudinal coupling* involves interaction through the diagonal elements without any energy transfer. This type of longitudinal noise causes random rotations of the Bloch vector around the $z$-axis, characterized by the *pure dephasing rate* $\Gamma_\varphi$.

Transverse noise can also lead to the loss of information about the relative phase. When the qubit is de-excited to $|0\rangle$, the knowledge of its previous superposition state is destroyed in the process. Therefore, the *transverse relaxation rate* $\Gamma_2$ is defined as the sum total [14]

$$\Gamma_2 \coloneqq \frac{\Gamma_1}{2} + \Gamma_\varphi. \tag{3.35}$$

Dealing with open systems, we turn (without further exposition) to the formalism describing statistical ensembles of quantum states. The density matrix for a pure state $|\psi\rangle = \alpha|0\rangle + \beta|1\rangle$ is given by

$$\rho = |\psi\rangle\langle\psi| = \begin{pmatrix} |\alpha|^2 & \alpha\beta^* \\ \alpha^*\beta & |\beta|^2 \end{pmatrix}. \tag{3.36}$$

In the Bloch-Redfield model of decoherence [29], the longitudinal and transverse noise cause the density matrix to evolve as [14]

$$\rho(t) = \begin{pmatrix} 1 - |\beta|^2 \mathrm{e}^{-\Gamma_2 t} & \alpha\beta^* \mathrm{e}^{-\Gamma_2 t} \\ \alpha^*\beta \mathrm{e}^{-\Gamma_2 t} & |\beta|^2 \mathrm{e}^{-\Gamma_1 t} \end{pmatrix}. \tag{3.37}$$

From the form of the Bloch-Redfield density matrix $\rho(t)$, we observe that even when performing a trivial identity operation – essentially doing nothing – the outcome deviates from the desired state. The magnitude of overlap between the desired state $\hat{U}_0$ and the actual outcome $\hat{U}$ is portrayed by *fidelity*. As a quantitative measure, the fidelity for gate $\hat{U}_0$ may be defined as: [30]

$$\mathcal{F}(t,\hat{U}_0) \coloneqq \left|\langle\psi|\hat{U}_0^\dagger\hat{U}(t)|\psi\rangle\right|^2, \tag{3.38}$$

where $|\psi\rangle$ is the initial state. To get rid of the dependence on $|\psi\rangle$ we can instead consider *average fidelity* given by

$$\overline{\mathcal{F}}(t,\hat{U}_0) \coloneqq \int \mathrm{d}\psi\left|\langle\psi|\hat{U}_0^\dagger\hat{U}(t)|\psi\rangle\right|^2, \tag{3.39}$$

where the integration is taken over the Bloch sphere. If we perform the identity gate $\hat{I}$ the actual outcome $\hat{U}(t)$ is then the operator of free evolution. The average fidelity can then be explicitly calculated as follows: [31]

$$\begin{aligned}\overline{\mathcal{F}}(t,\hat{I}) &= \int \mathrm{d}\psi\left|\langle\psi|\hat{I}\hat{U}(t)|\psi\rangle\right|^2 \\ &= \int \mathrm{d}\psi\langle\psi|\left(|\psi(t)\rangle\langle\psi(t)|\right)|\psi\rangle \\ &= \int \mathrm{d}\psi\langle\psi|\rho(t)|\psi\rangle,\end{aligned} \tag{3.40}$$

where we inserted the Bloch-Redfield density matrix in Eq. (3.37). With $|\psi\rangle = (\alpha,\,\beta)^{\mathrm{T}}$ a straightforward matrix multiplication combined with the normalization condition $|\beta|^2 = 1-|\alpha|^2$ gives

$$\overline{\mathcal{F}}(t,\hat{I}) = \int \mathrm{d}\psi\Big[|\alpha|^2 + (2|\alpha|^4 - 3|\alpha|^2 + 1)\mathrm{e}^{-\Gamma_1 t} - 2(|\alpha|^4 - |\alpha|^2)\mathrm{e}^{-\Gamma_2 t}\Big]. \tag{3.41}$$

Changing to the spherical coordinates with substitutions

$$\int \mathrm{d}\psi = \frac{1}{4\pi}\int \mathrm{d}\theta\mathrm{d}\phi\sin\theta, \quad \text{and} \quad |\alpha| = \cos^2\left(\frac{\theta}{2}\right), \tag{3.42}$$

the integral in Eq. (3.43) is evaluated to be

$$\overline{\mathcal{F}}(t,\hat{I}) = \frac{1}{2} + \frac{1}{6}\mathrm{e}^{-\Gamma_1 t} + \frac{1}{3}\mathrm{e}^{-\Gamma_2 t}. \tag{3.43}$$

The above expression for average fidelity provides the upper bound for the fidelity of any qubit gate under the influence of decoherence [30, 31]. To conclude we define for later sections the average *infidelity*

$$\overline{\mathcal{E}}(t,\hat{U}_0) \coloneqq 1 - \overline{\mathcal{F}}(t,\hat{U}_0), \tag{3.44}$$

which characterizes a magnitude of error of the operation.

# 4. Noisy subharmonic drive

This chapter focuses on the study of the subharmonic drive, a control scheme where the transmon is driven at a fraction of its resonant frequency. First, we demonstrate that driving the transmon at one-third of its frequency results in a Rabi rate proportional to the cube of the applied voltage. Next, we introduce voltage fluctuations to the drive amplitude and examine the resulting noisy subharmonic Hamiltonian. We conclude by calculating the decay rate and the average gate fidelity.

## 4.1 Subharmonic Hamiltonian

Separating the drive frequency from the qubit transition frequency would break the conflict between the qubit coherence and gate speed. Despite the apparent benefits exciting the qubit with off-resonant drive seems at first glance implausible. Our discussion in Section 2.7 suggests that driving a two-level system at off-resonant frequencies would only decrease the amplitude of Rabi oscillations. However, the full dynamics of the transmon can be obscured if not carefully examined. The contribution of typically suppressed fast-rotating terms becomes significant at subharmonic frequencies as they fascilitate multiphoton transitions. In this section, we derive the transmon Hamiltonian under a subharmonic drive in detail, following the original outline in [9]. We start with the complete transmon Hamiltonian:

$$\hat{H}_{\mathrm{T}} = \hbar\omega_p \hat{q}^\dagger \hat{q} + \hbar\frac{\alpha}{12}(\hat{q}^\dagger + \hat{q})^4, \tag{4.1}$$

where the Josephson plasma frequency $\omega_p = \sqrt{8E_C E_{\mathrm{J}}}$ and the anharmonicity $\alpha = -E_C$ were defined in Eq. (2.30). Coupling the qubit to a drive $\Omega(t)$ results in the following Hamiltonian[†]:

[†]Here, we use inductive coupling $(\hat{q}^\dagger + \hat{q})$ following the approach of [9], as opposed to the capacitive coupling $i(\hat{q}^\dagger - \hat{q})$ used in Section 2.7. Regardless of the type of coupling, the dynamics are equivalent.

$$\begin{aligned}\hat{H} &= \hat{H}_{\mathrm{T}} + \hat{H}_{\mathrm{d}}(t) \\ &= \hbar\omega_p \hat{q}^\dagger \hat{q} + \hbar\frac{\alpha}{12}(\hat{q}^\dagger + \hat{q})^4 + \hbar\Omega(t)(\hat{q}^\dagger + \hat{q}).\end{aligned} \tag{4.2}$$

The driving term can be cancelled by applying a displacement transformation $\hat{D}(t) = \mathrm{e}^{z(t)\hat{q}^\dagger - z^*(t)\hat{q}}$. With an appropriately chosen $z(t)$, the transformed Hamiltonian becomes

$$\hat{H}_{\mathrm{D}}/\hbar \coloneqq \omega_p \hat{q}^\dagger \hat{q} + \frac{\alpha}{12}\left(\hat{q}^\dagger + \hat{q} - z^*(t) - z(t)\right)^4, \tag{4.3}$$

up to a time-dependent scalar. For expositional clarity, these calculations are performed in Section A.1. There, we show that the driving terms vanish if $z(t)$ satisfies the following first-order non-homogeneous linear differential equation

$$\dot{z} + \mathrm{i}\omega_p z = \mathrm{i}\Omega(t). \tag{4.4}$$

It is straightforward to obtain the general solution

$$z(t) = \mathrm{e}^{-\mathrm{i}\omega_p t}\Big[\int_0^t \mathrm{d}\tau i \mathrm{e}^{\mathrm{i}\omega_p \tau}\Omega(\tau) + C\Big], \tag{4.5}$$

where $C = 0$ due to the initial condition. In the case of a single microwave drive at frequency $\omega_d$, we set

$$\Omega(t) = \begin{cases} \varepsilon(t)\mathrm{e}^{-\mathrm{i}\omega_d t} + \varepsilon^*(t)\mathrm{e}^{\mathrm{i}\omega_d t} & 0 < t < t_{\mathrm{gate}} \\ 0 & \text{otherwise} \end{cases} \tag{4.6}$$

where $\varepsilon(t)$ is the time-dependent amplitude experienced by the qubit, and $t_{\mathrm{gate}}$ is the gate time. For the capacitive coupling between the drive line and the qubit, $\varepsilon(t) = i\sqrt{\gamma}\beta(t)$, where $\gamma$ is the interaction strength and $\beta(t) \propto V$ is the drive amplitude of the input field. Here, $\gamma$ is determined by the circuit parameters, such as the coupling capacitance and transmission line impedance, while $\beta \propto V$ scales linearly with the applied voltage $V$ (for the explicit forms, see [13] and [32]).

Assuming that amplitude $\varepsilon(t)$ is slowly varying compared to the drive frequency, we approximate (4.5) as

$$\begin{aligned} z(t) &= \mathrm{e}^{-\mathrm{i}\omega_p t}\Big[\int_0^t \mathrm{d}t' i \mathrm{e}^{\mathrm{i}\omega_p \tau}\left(\varepsilon(\tau)\mathrm{e}^{-\mathrm{i}\omega_d \tau} + \varepsilon(\tau)^*\mathrm{e}^{\mathrm{i}\omega_d \tau}\right)\Big] \\ &\approx \frac{\varepsilon(t)}{\omega_p - \omega_d}\mathrm{e}^{-\mathrm{i}\omega_d t} + \frac{\varepsilon^*(t)}{\omega_p + \omega_d}\mathrm{e}^{\mathrm{i}\omega_d t}. \end{aligned} \tag{4.7}$$

Now, we find

$$\begin{aligned} z(t) + z^*(t) &= \left(\frac{1}{\omega_p - \omega_d} + \frac{1}{\omega_p + \omega_d}\right)\left(\varepsilon(t)\mathrm{e}^{-\mathrm{i}\omega_d t} + \varepsilon^*(t)\mathrm{e}^{\mathrm{i}\omega_d t}\right) \\ &= \frac{2\omega_p}{\omega_p^2 - \omega_d^2}\left(\varepsilon(t)\mathrm{e}^{-\mathrm{i}\omega_d t} + \varepsilon^*(t)\mathrm{e}^{\mathrm{i}\omega_d t}\right) \\ &= -\eta\mathrm{e}^{-\mathrm{i}\omega_d t} - \eta^*\mathrm{e}^{\mathrm{i}\omega_d t}, \end{aligned} \tag{4.8}$$

where in the last line we defined

$$\eta \coloneqq \frac{2\omega_p\varepsilon(t)}{\omega_d^2 - \omega_p^2}. \tag{4.9}$$

With obtained identities, the displaced Hamiltonian in (4.3) becomes

$$\hat{H}_\mathrm{D}/\hbar = \omega_p\hat{q}^\dagger\hat{q} + \frac{\alpha}{12}\left(\hat{q}^\dagger + \hat{q} + \eta\mathrm{e}^{-\mathrm{i}\omega_d t} + \eta^*\mathrm{e}^{\mathrm{i}\omega_d t}\right)^4 \tag{4.10}$$

We consider a drive frequency close to one-third of the qubit frequency $\omega_q = \omega_p + \alpha$ as defined in Eq. (2.30). Consequently, we set $\omega_d = \omega_q/3 + \delta$, where $\delta$ is the detuning between the drive frequency and the 1/3-subharmonic. Applying the unitary transformation $\hat{U}_\mathrm{R} = \mathrm{e}^{\mathrm{i}3\omega_d t\hat{q}^\dagger\hat{q}}$, we move to the rotating frame, where the Hamiltonian reads:

$$\hat{H}_\mathrm{R}/\hbar = (\omega_p - 3\omega_d)\hat{q}^\dagger\hat{q} + \frac{\alpha}{12}\left(\hat{q}^\dagger\mathrm{e}^{\mathrm{i}3\omega_d t} + \hat{q}\mathrm{e}^{-\mathrm{i}3\omega_d t} + \eta\mathrm{e}^{-\mathrm{i}\omega_d t} + \eta^*\mathrm{e}^{\mathrm{i}\omega_d t}\right)^4. \tag{4.11}$$

For additional details, refer to Section A.2. The second term in Eq. (4.11) can be expanded into a sum of individual terms of the form

$$\eta^m\eta^{*n}\sigma(\hat{q}^{\dagger i}\hat{q}^j)\mathrm{e}^{-\mathrm{i}(m-n-3i+3j)\omega_d t}, \tag{4.12}$$

where $\sigma$ applies some permutation of $i$ instances of $\hat{q}^\dagger$, and $j$ instances of $\hat{q}$ and the indices $i$, $j$, $m$, $n \in \mathbb{N}$ satisfy $i + j + m + n = 4$.

We can now apply the rotating wave approximation and discard all oscillating terms in the chosen frame. Only those terms that satisfy $m - n - 3i + 3j = 0$ are kept. Detailed discussion on these remaining terms is provided in Section A.3. The subharmonic Hamiltonian then takes the form

$$\hat{H}_\mathrm{R}^\mathrm{RWA}/\hbar \coloneqq (2\alpha|\eta|^2 - 3\delta)\hat{q}^\dagger\hat{q} + \frac{\alpha}{2}\hat{q}^\dagger\hat{q}^\dagger\hat{q}\hat{q} + \frac{\alpha}{3}(\eta^3\hat{q}^\dagger + \eta^{*3}\hat{q}). \tag{4.13}$$

Upon closer inspection, the Hamiltonian above closely resembles the transmon Hamiltonian under a resonant drive. The last two terms give the Kerr non-linearity and an effective drive of the strength proportional to $|\eta|^3$.

In the case of a resonant drive, the number operator is cancelled in the rotating frame. However, for the derived subharmonic Hamiltonian, there is an additional prefactor of $2\alpha|\eta|^2 - 3\delta$. This drive-dependent term induces a shift in the qubit frequency, known as the AC Stark shift. To counteract the AC-Stark shift we choose the drive detuning to be

$$\delta = \frac{2}{3}\alpha|\eta|^2, \tag{4.14}$$

reducing the subharmonic Hamiltonian in Eq. (4.13) to

$$\hat{H}_{\mathrm{R}}^{\mathrm{RWA}}/\hbar = \frac{\alpha}{2}\hat{q}^\dagger\hat{q}^\dagger\hat{q}\hat{q} + \frac{\alpha}{3}(\eta^3\hat{q}^\dagger + \eta^{*3}\hat{q}). \tag{4.15}$$

In this approach, the drive amplitude must remain approximately constant throughout the pulse. This requirement can be met using flat-top pulses [**?**]. By approximating the drive amplitude as constant, we set $2|\varepsilon(t)| \approx \Omega_{\mathrm{R}} = \mathrm{const}^*$, where $\Omega_{\mathrm{R}}$ is the Rabi angular frequency (see Section 2.7). Now, the subharmonic Rabi frequency reads

$$\Omega_{\mathrm{R}}^{\mathrm{sub}} = \frac{2}{3}\alpha|\eta|^3 = \frac{2}{3}\alpha\left(\frac{\Omega_{\mathrm{R}}\omega_p}{\omega_p^2 - \omega_d^2}\right)^3. \tag{4.16}$$

The cubic relationship between the subharmonic Rabi rate and the drive voltage gives the possibility to greatly increase the gate execution times by increasing the applied power incrementally. Another significant advantage of subharmonic driving is the ability to shield the qubit from decay by filtering out noise at its transition frequency.

Since the drive frequency differs from the qubit frequency, we can suppress the primary relaxation channel while still being able to drive the qubit.

## 4.2 Noisy subharmonic Hamiltonian

In this section, we investigate the effects of voltage fluctuations in the case of subharmonic driving. We use a semi-classical model, where a real random signal $\delta\Omega(t)$ is added to the drive strength. Thus, the transmon Hamiltonian under a noisy drive reads

*The factor of two is a result of defining the drive using complex exponentials instead of trigonometric functions

$$\hat{H}^{\delta\Omega} \coloneqq \hbar\omega_p \hat{q}^\dagger \hat{q} + \hbar\frac{\alpha}{12}(\hat{q}^\dagger + \hat{q})^4 + \hbar(\Omega(t) + \delta\Omega(t))(\hat{q}^\dagger + \hat{q}), \tag{4.17}$$

which corresponds to Eq. (4.2) with the substitution $\Omega(t) \to \Omega(t) + \delta\Omega(t)$. We assume that $\delta\Omega(t)$ is a stationary, centered process, allowing us to utilize the tools from Chapter 3. Applying the displacement transformation from the previous section, we get

$$\begin{aligned}\hat{H}_{\mathrm{D}}^{\delta\Omega}\hbar = \omega_p \hat{q}^\dagger \hat{q} + \frac{\alpha}{12}\left(\hat{q}^\dagger + \hat{q} - z^*(t) - z(t)\right)^4 \\ + (\Omega(t) + \delta\Omega(t) + \mathrm{i}\dot{z} - \omega_p z)\hat{q}^\dagger + h.c.\end{aligned} \tag{4.18}$$

Similar to Eq. (4.4), the driving terms disappear if we impose the condition:

$$\dot{z} + \mathrm{i}\omega_p z = \mathrm{i}\Omega(t) + \mathrm{i}\delta\Omega(t). \tag{4.19}$$

Due to linearity, we can separate $z(t)$ into a deterministic part and a stochastic part, $z(t) \to z(t) + Z(t)$. This decomposition yields two differential equations: one ordinary and one random.

$$\dot{z} + \mathrm{i}\omega_p z = \mathrm{i}\Omega(t), \tag{4.20}$$

$$\dot{Z} + \mathrm{i}\omega_p Z = \mathrm{i}\delta\Omega(t). \tag{4.21}$$

We handle the ODE as in the previous section by considering the drive $\Omega(t)$ in Eq. (4.6). Consequently, the displaced Hamiltonian in Eq. (4.18) takes the form

$$\hat{H}^D_{\mathrm{noisy}}/\hbar = \omega_p \hat{q}^\dagger \hat{q} + \frac{\alpha}{12}\left(\hat{q}^\dagger + \hat{q} + \eta \mathrm{e}^{-\mathrm{i}\omega_d t} + \eta^* \mathrm{e}^{\mathrm{i}\omega_d t} - Z(t) - Z^*(t)\right)^4. \tag{4.22}$$

We can simplify our work significantly by observing that only the real part of $Z(t)$ appears in the Hamiltonian above. Hence, we express $Z(t)$ as $Z(t) = X(t) + \mathrm{i}Y(t)$, where $X(t)$ and $Y(t)$ are real random functions. This modifies Eq. (4.21) to:

$$\dot{X} + \mathrm{i}\dot{Y} + \omega_p(\mathrm{i}X - Y) = \mathrm{i}\delta\Omega(t). \tag{4.23}$$

The interactive part of the Hamiltonian in Eq. (4.17) indicates an inductive coupling through flux operator $\hat{\Phi} \propto (\hat{q}^\dagger + \hat{q})$. As Hamiltonian must be self-adjoint, $\delta\Omega(t)$ can be taken to be real and Eq. (4.23) may be decoupled to give

$$\ddot{X} + \omega_p^2 X = \omega_p \delta\Omega(t). \tag{4.24}$$

However, we are interested in the capacitive coupling of the qubit to the transmission line. Then, the semi-classical voltage fluctuations couple to the qubit through charge operator $\hat{Q} \propto \mathrm{i}(\hat{q}^\dagger - \hat{q})$. Replacing $\delta\Omega(t)(\hat{q}^\dagger + \hat{q})$ with $\mathrm{i}\delta\Omega(t)(\hat{q}^\dagger - \hat{q})$ in Eq. (4.17) yields the same derivation just with a substitution $\delta\Omega(t) \to \mathrm{i}\delta\Omega(t)$. Thus, instead of Eq. (4.23) we consider

$$\dot{X} + \mathrm{i}\dot{Y} + \omega_p(\mathrm{i}X - Y) = -\delta\Omega(t). \tag{4.25}$$

Again assuming $\delta\Omega(t)$ is a real random function, decoupling Eq. (4.25) gives instead:

$$\ddot{X} + \omega_p^2 X = -\delta\dot{\Omega}(t), \tag{4.26}$$

From Eqs. (4.24) and (4.26) we observe that for both types of coupling, the response $X(t)$ follows the equation of an undamped harmonic oscillator. The driving force is $\delta\Omega(t)$ in the case of inductive coupling, and $\delta\dot{\Omega}(t)$ in the case of capacitive coupling, reflecting the relationship $\dot{\Phi}(t) = V(t)$.

Continuing with the latter case, we derive the power spectral density of $X(t)$ with the tools of harmonic analysis presented in Sections 3.2 and 3.3. Taking the Fourier transform of Eq. (4.26), we obtain

$$S_{XX}[\omega] = \frac{\omega^2}{(\omega_p^2 - \omega^2)^2} S_{\Omega\Omega}[\omega], \tag{4.27}$$

where $S_{XX}$ and $S_{\Omega\Omega}$ are the power spectral densities of $X(t)$ and $\delta\Omega(t)$, respectively. The power spectrum of $X(t)$ has a second order pole at resonance $\omega = \omega_p$ and we will address this problematic feature later.

We finally return to the Hamiltonian in Eq. (4.18), which can be rewritten as

$$\hat{H}_{\mathrm{D}}^{\delta\Omega}/\hbar = \omega_p \hat{q}^\dagger \hat{q} + \frac{\alpha}{12}\left(\hat{q}^\dagger + \hat{q} + \eta \mathrm{e}^{-\mathrm{i}\omega_d t} + \eta^* \mathrm{e}^{\mathrm{i}\omega_d t} - 2X(t)\right)^4, \tag{4.28}$$

where we made a substitution $Z(t) + Z^*(t) = 2X(t)$. We proceed as in the previous section by transforming to the frame rotating at $3\omega_d$, giving:

$$\hat{H}_{\mathrm{R}}^{\delta\Omega}/\hbar = (\omega_p - 3\omega_d)\hat{q}^\dagger \hat{q} + \frac{\alpha}{12}\left(\hat{q}^\dagger \mathrm{e}^{\mathrm{i}3\omega_d t} + \hat{q}\mathrm{e}^{-\mathrm{i}3\omega_d t} + \eta \mathrm{e}^{-\mathrm{i}\omega_d t} + \eta^* \mathrm{e}^{\mathrm{i}\omega_d t} - 2X(t)\right)^4 \tag{4.29}$$

Assuming the noise term is small, we expand the product keeping the noise term only in the first order

$$\begin{aligned}\hat{H}_{\mathrm{R}}^{\delta\Omega}/\hbar &\approx (\omega_p - 3\omega_d)\hat{q}^\dagger\hat{q} + \frac{\alpha}{12}\left(\hat{q}^\dagger \mathrm{e}^{\mathrm{i}3\omega_d t} + \hat{q}\mathrm{e}^{-\mathrm{i}3\omega_d t} + \eta\mathrm{e}^{-\mathrm{i}\omega_d t} + \eta^*\mathrm{e}^{\mathrm{i}\omega_d t}\right)^4 \\ &\quad - \frac{2\alpha}{3}X(t)\left(\hat{q}^\dagger \mathrm{e}^{\mathrm{i}3\omega_d t} + \hat{q}\mathrm{e}^{-\mathrm{i}3\omega_d t} + \eta\mathrm{e}^{-\mathrm{i}\omega_d t} + \eta^*\mathrm{e}^{\mathrm{i}\omega_d t}\right)^3 \\ &= \hat{H}_{\mathrm{R}}/\hbar - \frac{2\alpha}{3}X(t)\left(\hat{q}^\dagger \mathrm{e}^{\mathrm{i}3\omega_d t} + \hat{q}\mathrm{e}^{-\mathrm{i}3\omega_d t} + \eta\mathrm{e}^{-\mathrm{i}\omega_d t} + \eta^*\mathrm{e}^{\mathrm{i}\omega_d t}\right)^3, \end{aligned} \tag{4.30}$$

where we reintroduced the Hamiltonian $\hat{H}_{\mathrm{R}}$ from (4.11). Just as before, we discard the rotating terms from $\hat{H}_{\mathrm{R}}$, resulting in $\hat{H}_{\mathrm{R}}^{\mathrm{RWA}}$ as given in (2.31).

In the following section, we derive the longitudinal relaxation rate $\Gamma_1$ introduced in Section 3.5. In anticipation of the use of the time-dependent perturbation theory, we write the noisy subharmonic Hamiltonian as

$$\begin{aligned}\hat{H}_{\mathrm{R}}^{\delta\Omega,\mathrm{RWA}}/\hbar &\coloneqq \hat{H}_{\mathrm{R}}^{\mathrm{RWA}}/\hbar - \frac{2\alpha}{3}X(t)\left(\hat{q}^\dagger \mathrm{e}^{\mathrm{i}3\omega_d t} + \hat{q}\mathrm{e}^{-\mathrm{i}3\omega_d t} + \eta\mathrm{e}^{-\mathrm{i}\omega_d t} + \eta^*\mathrm{e}^{\mathrm{i}\omega_d t}\right)^3 \\ &= \hat{H}_0/\hbar + \delta\hat{H}(t)/\hbar, \end{aligned} \tag{4.31}$$

where we defined

$$\hat{H}_0/\hbar \coloneqq \frac{\alpha}{12}\hat{q}^\dagger\hat{q}^\dagger\hat{q}\hat{q}, \tag{4.32}$$

$$\delta\hat{H}(t)/\hbar \coloneqq \frac{\alpha}{3}(\eta^3\hat{q}^\dagger + \eta^{*3}\hat{q}) - \frac{2\alpha}{3}X(t)\left(\hat{q}^\dagger \mathrm{e}^{\mathrm{i}3\omega_d t} + \hat{q}\mathrm{e}^{-\mathrm{i}3\omega_d t} + \eta\mathrm{e}^{-\mathrm{i}\omega_d t} + \eta^*\mathrm{e}^{\mathrm{i}\omega_d t}\right)^3. \tag{4.33}$$

We note that the form of $\hat{H}_0$ indicates the drive detuning to be fixed as in Eq. (4.14).

## 4.3 Calculating the decay rate

In this section we calculate the longitudinal relaxation rate $\Gamma_1$ as defined in Eq. (4.49). At low temperatures, the decay rate is dominated by $\Gamma_{1\downarrow}$, which characterizes the transition from the excited state $|1\rangle$ to the ground state $|0\rangle$ due to noise.

We calculate the transition rate using the time-dependent perturbation theory in the leading order. The evolution of the state function $|\psi(t)\rangle_I$ in interaction picture takes the form

$$|\psi(t)\rangle_I \approx |\psi(0)\rangle_I - \frac{i}{\hbar}\int_0^t d\tau \delta\hat{H}_I(\tau)|\psi(0)\rangle_I, \tag{4.34}$$

where $\delta\hat{H}_I(t)$ is the interaction picture representation of $\delta\hat{H}(t)$ in Eq. (4.33) given by

$$\begin{aligned}\delta\hat{H}_I(t) &= \mathrm{e}^{\mathrm{i}\hat{H}_0 t/\hbar}\delta\hat{H}(t)\mathrm{e}^{-\mathrm{i}\hat{H}_0 t/\hbar} \\ &= \mathrm{e}^{\mathrm{i}\frac{\alpha}{2}\hat{q}^\dagger\hat{q}^\dagger\hat{q}\hat{q}t}\delta\hat{H}(t)\mathrm{e}^{-\mathrm{i}\frac{\alpha}{2}\hat{q}^\dagger\hat{q}^\dagger\hat{q}\hat{q}t}.\end{aligned} \tag{4.35}$$

Since in our approach $\hat{H}_0$ contains only the non-linear Kerr term, the ground and excited states are degenerate, leading to

$$\mathrm{e}^{\mathrm{i}\frac{\alpha}{2}\hat{q}^\dagger\hat{q}^\dagger\hat{q}\hat{q}t}|e\rangle = |e\rangle, \quad \text{and} \quad \mathrm{e}^{\mathrm{i}\frac{\alpha}{2}\hat{q}^\dagger\hat{q}^\dagger\hat{q}\hat{q}t}|g\rangle = |g\rangle. \tag{4.36}$$

The noise term $\delta\hat{H}(t)$ in Eq. (4.33) can now be expanded and we highlight those individual terms that are relevant for the first-order dynamics. These terms have one $\hat{q}$ more than $\hat{q}^\dagger$ and as such do not vanish upon taking the inner product.

$$\begin{aligned}&X(t)\left(\hat{q}^\dagger\mathrm{e}^{\mathrm{i}3\omega_d t} + \hat{q}\mathrm{e}^{-\mathrm{i}3\omega_d t} + \eta\mathrm{e}^{-\mathrm{i}\omega_d t} + \eta^*\mathrm{e}^{\mathrm{i}\omega_d t}\right)^3 \\ &\quad= X(t)\mathrm{e}^{-\mathrm{i}3\omega_d t}\Big[3\left(\eta\mathrm{e}^{-\mathrm{i}\omega_d t} + \eta^*\mathrm{e}^{\mathrm{i}\omega_d t}\right)^2\hat{q} + (\hat{q}^\dagger\hat{q}\hat{q} + \hat{q}\hat{q}^\dagger\hat{q} + \hat{q}\hat{q}\hat{q}^\dagger) + \ldots\Big] \\ &\quad= 3X(t)\mathrm{e}^{-\mathrm{i}3\omega_d t}\Big[\left(\eta\mathrm{e}^{-\mathrm{i}\omega_d t} + \eta^*\mathrm{e}^{\mathrm{i}\omega_d t}\right)^2\hat{q} + \hat{q} + \ldots\Big].\end{aligned} \tag{4.37}$$

With these relations, the transition amplitude between the excited state to the ground state is given by

$$\begin{aligned}\alpha(t) &= \langle g\,|\,\psi(t)\rangle_I \\ &\approx \langle g\,|\,e\rangle - \frac{\mathrm{i}}{\hbar}\int_0^t d\tau\langle g|\delta\hat{H}_I(\tau)|e\rangle \\ &= -\mathrm{i}\int_0^t d\tau\langle g|\Big\{\frac{\alpha}{3}(\eta^3\hat{q}^\dagger + \eta^{*3}\hat{q}) \\ &\quad - 2\alpha X(\tau)\mathrm{e}^{-\mathrm{i}3\omega_d\tau}\Big[\left(\eta\mathrm{e}^{-\mathrm{i}\omega_d\tau} + \eta^*\mathrm{e}^{\mathrm{i}\omega_d\tau}\right)^2\hat{q} + \hat{q} + \ldots\Big]\Big\}|e\rangle \\ &= -\mathrm{i}\alpha\int_0^t d\tau\Big\{\frac{1}{3}\eta^{*3} - 2X(\tau)\mathrm{e}^{-\mathrm{i}3\omega_d\tau}\Big[\left(\eta\mathrm{e}^{-\mathrm{i}\omega_d\tau} + \eta^*\mathrm{e}^{\mathrm{i}\omega_d\tau}\right)^2 + 1\Big]\Big\}.\end{aligned} \tag{4.38}$$

The transition probability respectively becomes

$$\begin{aligned}\alpha^\dagger(t)\alpha(t) = \alpha^2\int_0^t\int_0^t d\tau_1 d\tau_2\Big\{&\frac{1}{9}\eta(\tau_1)\eta^*(\tau_2) \\ &+ \Big(2X(\tau_1)\mathrm{e}^{\mathrm{i}3\omega_d\tau_1}\Big[\left(\eta(\tau_1)\mathrm{e}^{-\mathrm{i}\omega_d\tau_1} + \eta^*(\tau_1)\mathrm{e}^{\mathrm{i}\omega_d\tau_1}\right)^2 + 1\Big] \\ &\times 2X(\tau_2)\mathrm{e}^{-\mathrm{i}3\omega_d\tau_2}\Big[\left(\eta(\tau_2)\mathrm{e}^{-\mathrm{i}\omega_d\tau_2} + \eta^*(\tau_2)\mathrm{e}^{\mathrm{i}\omega_d\tau_2}\right)^2 + 1\Big]\Big) + \ldots\Big\},\end{aligned} \tag{4.39}$$

where we highlighted the time dependence of the prefactors $\eta$. We also left out the terms that are linear in $X(\tau)$ as these will vanish in the next step. Taking the ensemble average (see Section 3.1), we obtain the average transition probability

$$\begin{aligned}\langle\alpha^\dagger(t)\alpha(t)\rangle &= \alpha^2\int_0^t\int_0^t d\tau_1 d\tau_2 \frac{1}{9}\eta(\tau_1)\eta^*(\tau_2)\\ &\quad+\alpha^2\int_0^t\int_0^t d\tau_1 d\tau_2\Big\{4\langle X(\tau_1)X(\tau_2)\rangle \mathrm{e}^{\mathrm{i}3\omega_d(\tau_1-\tau_2)}\\ &\quad\times\Big[\Big(\eta(\tau_1)\mathrm{e}^{-\mathrm{i}\omega_d\tau_1}+\eta^*(\tau_1)\mathrm{e}^{\mathrm{i}\omega_d\tau_1}\Big)^2+1\Big]\Big[\Big(\eta(\tau_2)\mathrm{e}^{-\mathrm{i}\omega_d\tau_2}+\eta^*(\tau_2)\mathrm{e}^{\mathrm{i}\omega_d\tau_2}\Big)^2+1\Big]\Big\}\\ &\coloneqq P_\Omega(t)+P_{\delta\Omega}(t).\end{aligned} \tag{4.40}$$

From the above form, we see that the first-order transition probabilities $P_\Omega(t)$, due to the pure driving field, and $P_{\delta\Omega}(t)$, due to the fluctuations, are additive. Since we are only interested in decay caused by decoherence, we will focus on the latter quantity

$$\begin{aligned}P_{\delta\Omega}(t) \approx \alpha^2\int_0^t\int_0^t d\tau_1 d\tau_2\Big\{&4\langle X(\tau_1)X(\tau_2)\rangle \mathrm{e}^{\mathrm{i}3\omega_d(\tau_1-\tau_2)}\\ &\times\Big[\Big(\eta\mathrm{e}^{-\mathrm{i}\omega_d\tau_1}+\eta^*\mathrm{e}^{\mathrm{i}\omega_d\tau_1}\Big)^2+1\Big]\Big[\Big(\eta\mathrm{e}^{-\mathrm{i}\omega_d\tau_2}+\eta^*\mathrm{e}^{\mathrm{i}\omega_d\tau_2}\Big)^2+1\Big]\Big\},\end{aligned} \tag{4.41}$$

where we omitted the the time dependence of $\eta$ and from now on approximate it as constant. Since $\langle X(\tau_1)X(\tau_2)\rangle$ represents the correlation function of the response $X(\tau)$, we can combine the Wiener-Khinchin theorem (see Eq. (3.17)) with Eq. (4.27) to obtain:

$$\langle X(\tau_1)X(\tau_2)\rangle = \int_{-\infty}^{\infty}\frac{\mathrm{d}\omega}{2\pi}\frac{\omega^2}{(\omega_p^2-\omega^2)^2}S_{\Omega\Omega}[\omega]\mathrm{e}^{-\mathrm{i}\omega(\tau_1-\tau_2)}. \tag{4.42}$$

The integral above does not converge due to the presence of a second-order pole, making it analytically challenging to handle. By comparing the integrand in this formula with the power spectral density of a damped harmonic oscillator in Eq. (4.27), we find that they are identical when the damping coefficient is set to zero.

One might consider adding an infinitesimal damping term to Eq. (4.26) in the form of $\mathrm{i}\epsilon X$, which shifts the poles off the real axis. However, as shown by the correlation function of a damped oscillator in Eq. (3.25), the residues become proportional to $1/\epsilon$, causing the amplitude to diverge as $\epsilon \to 0$. Consequently, the correlation function oscillates instead of exhibiting exponential decay.

To proceed, we assume that the qubit is coupled to a filter that has a stop band at the resonant frequency $\omega_p$, effectively filtering it out. As such we redefine the power spectral density in Eq. (4.27) to be

$$S^H_{\Omega\Omega}[\omega] \coloneqq S_{\Omega\Omega}[\omega]H[\omega], \tag{4.43}$$

where $H$ is some filter function such that $H[\omega_p] = 0$. As the processes $X(\tau)$ is by assumption stationary the correlation function in Eq. (4.42) depends only on the time difference. Therefore, we make a change of variables in Eq. (4.41), $\tau^- = \tau_1 - \tau_2$ and $\tau^+ = (\tau_1 + \tau_2)/2$, and we get

$$\begin{aligned} P_{\delta\Omega}(t) = 4\alpha^2 \int_0^t d\tau^+ \int_{-b(\tau^+)}^{b(\tau^+)} d\tau^- \langle X(\tau^+ + \frac{\tau^-}{2}) X(\tau^+ - \frac{\tau^-}{2}) \rangle \\ \times \mathrm{e}^{\mathrm{i}3\omega_d\tau^-} \Big[ \Big( \eta \mathrm{e}^{-\mathrm{i}\omega_d(\tau^+ + \tau^-/2)} + \eta^* \mathrm{e}^{\mathrm{i}\omega_d(\tau^+ + \tau^-/2)} \Big)^2 + 1 \Big] \\ \times \Big[ \Big( \eta \mathrm{e}^{-\mathrm{i}\omega_d(\tau^+ - \tau^-/2)} + \eta^* \mathrm{e}^{\mathrm{i}\omega_d(\tau^+ - \tau^-/2)} \Big)^2 + 1 \Big], \end{aligned} \tag{4.44}$$

where the Jacobian of the transformation is unity and the integral bound $b(\tau^+)$ reads

$$b(\tau^+) = \begin{cases} \tau^+ & \text{if } \tau^+ < t/2, \\ t - \tau^+ & \text{if } \tau^+ > t/2. \end{cases} \tag{4.45}$$

Expanding the product in Eq. (4.44) gives numerous terms. Writing only those that do not oscillate as a function of $\tau^+$, we obtain:

$$\begin{aligned} P_{\delta\Omega}(t) = 4\alpha^2 \int_0^t d\tau^+ \int_{-b(\tau^+)}^{b(\tau^+)} d\tau^- \langle X(\tau^-) X(0) \rangle \\ \times \Big[ |\eta|^4 \mathrm{e}^{\mathrm{i}\omega_d\tau^-} + (2|\eta|^2 + 1)^2 \mathrm{e}^{\mathrm{i}3\omega_d\tau^-} + |\eta|^4 \mathrm{e}^{\mathrm{i}5\omega_d\tau^-} + \ldots \Big]. \end{aligned} \tag{4.46}$$

Next we assume that the correlation function of $X(\tau)$ has a finite but small correlation time $\tau_c$. Then, for $\tau^- \gg \tau_c$, the correlation function decays rapidly to zero and we may extend the bound $b(\tau^+)$ to infinity [33]. With these assumptions, we get

$$\begin{aligned} P_{\delta\Omega}(t) \approx 4\alpha^2 \int_0^t d\tau^+ \int_{-\infty}^{\infty} d\tau^- \langle X(\tau^-) X(0) \rangle \\ \times \Big[ |\eta|^4 \mathrm{e}^{\mathrm{i}\omega_d\tau^-} + (2|\eta|^2 + 1)^2 \mathrm{e}^{\mathrm{i}3\omega_d\tau^-} + |\eta|^4 \mathrm{e}^{\mathrm{i}5\omega_d\tau^-} + \ldots \Big], \end{aligned} \tag{4.47}$$

where the inner integral is just a Fourier transform of the correlation function. The inverse of Eq. (4.42) gives

$$P_{\delta\Omega}(t) \approx 4\alpha^2 \int_0^t d\tau^+ \Big[ |\eta|^4 S_{XX}[\omega_d] + (2|\eta|^2 + 1)^2 S_{XX}[3\omega_d] + |\eta|^4 S_{XX}[5\omega_d] + \ldots \Big]. \tag{4.48}$$

Since the omitted oscillating terms are expected to average out, the probability of decay increases linearly with time. Thus, we find the decay rate to be

$$\Gamma_{1\downarrow} = 4\alpha^2\Big[|\eta|^4\left(S_{XX}[\omega_d] + S_{XX}[5\omega_d]\right) + (2|\eta|^2+1)^2 S_{XX}[3\omega_d]\Big]. \tag{4.49}$$

Substituting the power spectral density from Eq. (4.27) gives

$$\begin{aligned}\Gamma_{1\downarrow} = 4\alpha^2\Bigg[|\eta|^4\left(\frac{\omega_d^2}{(\omega_p^2-\omega_d^2)^2}S^H_{\Omega\Omega}[\omega_d] + \frac{(5\omega_d)^2}{(\omega_p^2-(5\omega_d)^2)^2}S^H_{\Omega\Omega}[5\omega_d]\right)\\ + (2|\eta|^2+1)^2\frac{(3\omega_d)^2}{(\omega_p^2-(3\omega_d)^2)^2}S^H_{\Omega\Omega}[3\omega_d]\Bigg],\end{aligned} \tag{4.50}$$

where $S^H_{\Omega\Omega}$ is the filtered spectral density from Eq. (4.43). The term on the second line can be simplified by recalling that we had fixed the detuning such that $2\alpha|\eta|^2 = 3\delta$. Combining this with relations $\delta = \omega_d - \omega_q/3$ and $\omega_p = \omega_q - \alpha$, gives

$$\begin{aligned}\frac{(2|\eta|^2\alpha+\alpha)^2}{(\omega_p^2-(3\omega_d)^2)^2} &= \frac{(3\omega_d-\omega_q+\alpha)^2}{(\omega_p+3\omega_d)^2(\omega_p-3\omega_d)^2}\\ &= \frac{1}{(\omega_p+3\omega_d)^2},\end{aligned} \tag{4.51}$$

which reduces the transition rate to

$$\Gamma_{1\downarrow} = 4\alpha^2\omega_d^2|\eta|^4\left(\frac{S^H_{\Omega\Omega}[\omega_d]}{(\omega_p^2-\omega_d^2)^2} + \frac{25S^H_{\Omega\Omega}[5\omega_d]}{(\omega_p^2-25\omega_d^2)^2}\right) + \frac{36\omega_d^2}{(\omega_p+3\omega_d)^2}S^H_{\Omega\Omega}[3\omega_d]. \tag{4.52}$$

For small $|\eta|$, we could directly approximate $3\omega_d \approx \omega_q$ but as the actual relationship $3\omega_d = \omega_q + 3\delta$ depends on $3\delta = 2\alpha|\eta|^2$, we proceed with caution. Expanding the first two terms in the Taylor series gives the leading order of $|\eta|^4$. However, the third term also has lower power dependencies and can be expanded as

$$\begin{aligned}\frac{\omega_d^2}{(\omega_p+3\omega_d)^2} &= \frac{1}{9}\frac{(\omega_q+2\alpha|\eta|^2)^2}{(\omega_p+\omega_q+2\alpha|\eta|^2)^2}\\ &= \frac{1}{9}\Big[\frac{\omega_q^2}{(\omega_q+\omega_p)^2} + \frac{4\alpha\omega_p\omega_q}{(\omega_q+\omega_p)^3}|\eta|^2 + \frac{4\alpha^2(\omega_p^2-2\omega_p\omega_q)}{(\omega_q+\omega_p)^4}|\eta|^4 + \mathcal{O}(|\eta|^6)\Big]\\ &\approx \frac{1}{36}\Big[1 + \frac{2\alpha}{\omega_q}|\eta|^2 - \frac{\alpha^2}{\omega_q^2}|\eta|^4 + \mathcal{O}(|\eta|^6)\Big],\end{aligned} \tag{4.53}$$

where in the last line we approximated $\omega_p \approx \omega_q$ as the anharmonicity $\alpha$ is small. We note that since $\alpha$ is negative, the resulting corrections decrease the contribution to the decay at $3\omega_d$. Substituting the above expansion to Eq. (4.52), we can now approximate $3\omega_d \approx \omega_q$ and obtain:

$$\Gamma_{1\downarrow} = 9\frac{\alpha^2}{\omega_q^2}|\eta|^4\left(\frac{S^H_{\Omega\Omega}[\omega_q/3]}{16} + \frac{25S^H_{\Omega\Omega}[5\omega_q/3]}{64}\right) + \left[1 + \frac{2\alpha}{\omega_q}|\eta|^2 - \frac{\alpha^2}{\omega_q^2}|\eta|^4\right]S^H_{\Omega\Omega}[\omega_q]. \quad (4.54)$$

The above expression emphasizes a term that is independent of $|\eta|$ and represents spontaneous decay at $\omega_q$. Assuming $\delta\Omega(t)$ is proportional to voltage fluctuations $\delta V(t)$, we write

$$\delta\Omega(t) = g\delta V(t), \quad \text{and} \quad S^H_{\Omega\Omega}[\omega] = g^2 S_{VV}[\omega], \quad (4.55)$$

where $g$ is the coupling constant and $S_{VV}$ is the spectral density of quantum voltage noise as defined in Eq. (3.29). We have also omitted the filter function $H$ with the understanding that certain frequencies may be filtered out.

Since $\delta\Omega(t)$ is a real random variable, the power spectrum must be symmetric. Therefore, it is appropriate to use the symmetrized power spectrum in Eq. (3.30). However, if $\delta\Omega(t)$ is considered a quantum operator in the noise's Hilbert space, we could argue that the use of the asymmetric Nyquist spectrum is justified, assuming the derivation so far remains valid. It is interesting to note that even when treating $\delta\Omega(t)$ as an operator in Eq. (4.21), we could still decompose the solution $\hat{Z}$ into Hermitian $\hat{X}$ and anti-Hermitian $\hat{Y}$ parts, yielding the same equation Eq. (4.26) for $\hat{X}$. In either case, in the quantum limit, both the symmetrized form

$$S_{VV}[\omega] + S_{VV}[-\omega] = 2S^+_{VV}[\omega], \quad (4.56)$$

where $S^+_{VV}$ is defined in Eq. (3.30), and the quantum Nyquist spectral density in Eq. (3.29), converge to the same limit at positive frequencies. Therefore, at low temperatures and high frequencies, we can use

$$S_{VV}[\omega] = 2Z_c\hbar\omega, \quad \omega > 0, \quad (4.57)$$

in both cases. The final form for the decay rate is given by:

$$\begin{aligned}\Gamma_{1\downarrow} &= 3\frac{\alpha^2}{\omega_q}|\eta|^4 Z_c\hbar g^2\left(\frac{1}{8} + \frac{125}{32}\right) + 2Z_c\hbar g^2\left[\omega_q + 2\alpha|\eta|^2 - \frac{\alpha^2}{\omega_q}|\eta|^4\right] \\ &= Z_c\hbar g^2\left(\frac{323}{32}\frac{\alpha^2}{\omega_q}|\eta|^4 + 4\alpha|\eta|^2 + 2\omega_q\right) \\ &\approx Z_c\hbar g^2\left(10\frac{\alpha^2}{\omega_q}|\eta|^4 + 4\alpha|\eta|^2 + 2\omega_q\right). \end{aligned} \quad (4.58)$$

If we filter out the qubit frequency $3\omega_d$, we have

$$\Gamma_{1\downarrow}^{\mathrm{F}(3)} = \frac{387}{32} Z_c \hbar g^2 \frac{\alpha^2}{\omega_q} |\eta|^4 \approx 12 Z_c \hbar g^2 \frac{\alpha^2}{\omega_q} |\eta|^4. \tag{4.59}$$

where the super script F is the short hand for the filter. It is interesting to note that filtering out $3\omega_d$ actually increases the coefficient of $|\eta|^4$. By filtering out both $3\omega_d$ and $5\omega_d$ and retaining only the drive frequency $\omega_d \approx \omega_q/3$, we instead obtain:

$$\Gamma_{1\downarrow}^{\mathrm{F}(3,5)} = \frac{3}{8} Z_c \hbar g^2 \frac{\alpha^2}{\omega_q} |\eta|^4. \tag{4.60}$$

Comparing transition rates $\Gamma_{1\downarrow}$ and $\Gamma_{1\downarrow}^{\mathrm{F}(3,5)}$, we see that filtering both frequencies reduces the coefficients fourth-order terms, $|\eta|^4$ by 96 %. The largest contributor to these terms in $\Gamma_{1\downarrow}$ is the decay at $5\omega_d$. Most importantly, filtering out the qubit frequency $3\omega_d$ protects the qubit from spontaneous decay that is independent of the drive.

Rewriting Eq. (4.60) as a function subharmonic Rabi rate $\Omega_{\mathrm{R}}^{\mathrm{sub}}$ in Eq. (4.16), we have

$$\Gamma_{1\downarrow}^{\mathrm{F}(3,5)} = \frac{9\sqrt[3]{12}}{32} Z_c \hbar g^2 \frac{\alpha^{2/3}}{\omega_q} \left(\Omega_{\mathrm{R}}^{\mathrm{sub}}\right)^{4/3}. \tag{4.61}$$

$$\tag{4.62}$$

Lastly, analyzing the decay rate in Eq. (4.49), we note that a portion of the relaxation occurs at $5\omega_q/3$ due to the absorption of two $\omega_q/3$ photons and the emission of a single $5\omega_q/3$ photon. This third decay channel was not anticipated before the calculation.

## 4.4 Average fidelity of the subharmonic drive

In this section, we calculate the gate fidelity of the subharmonic drive pulse as a function of the mean photon number following the supplemental material of [34]. We use the $\pi$-pulse as an example, which has the gate length

$$t_{\mathrm{g}} = \frac{\pi}{\Omega_R^{\mathrm{sub}}}. \tag{4.63}$$

Multiplying the gate length $t_{\mathrm{g}}$ together with Eq. (4.61), gives

$$\Gamma_{1\downarrow}^{\Theta(3,5)} t_{\mathrm{g}} = \frac{9\pi}{16} Z_c \hbar g^2 \frac{\alpha}{\omega_q} |\eta|. \tag{4.64}$$

The driving strength can be rewritten as

$$2|\varepsilon(t)| = 2gV = gV_{\mathrm{p}}, \tag{4.65}$$

where $g$ is the coupling constant, $V$ is voltage amplitude and $V_{\mathrm{p}}$ is *peak-to-peak* voltage. Writing the average power requirement $P$ as

$$P = \frac{1}{8}\frac{V_{\mathrm{p}}^2}{Z_c}, \tag{4.66}$$

we can approximate the mean photon number $\overline{n}$ during a $\pi$-pulse with

$$\overline{n} = \frac{Pt_g}{\hbar\omega_d}. \tag{4.67}$$

Combining the above equation with Eqs. (4.63) and (4.66), we obtain the inverse relationship between $\eta$ and mean photon number:

$$\begin{aligned}\overline{n} &= \frac{3}{16}\frac{\pi}{\hbar\alpha\omega_d Z_c}\left(\frac{\omega_p^2-\omega_d^2}{g\omega_p}\right)^2\frac{1}{|\eta|} \\ &\approx \frac{4\pi}{9}\frac{\omega_q}{\hbar\alpha Z_c g^2}\frac{1}{|\eta|},\end{aligned} \tag{4.68}$$

where we approximated $\omega_d \approx \omega_q/3$. Equation (4.64) can be then rewritten as

$$\Gamma_{1\downarrow}^{\Theta(3,5)} t_{\mathrm{g}} = \frac{\pi^2}{2}\frac{1}{\overline{n}}. \tag{4.69}$$

In Section 3.5 we derived the average infidelity of an gate operation due to decoherence to be

$$\begin{aligned}\overline{\mathcal{E}}(t_g) &= 1 - \overline{F}(t_g) \\ &= 1 - \frac{1}{6}(3 + \mathrm{e}^{-\Gamma_1 t_g} + 2\mathrm{e}^{-\Gamma_2 t_g}).\end{aligned} \tag{4.70}$$

where $\Gamma_1$ and $\Gamma_2$ is the longitudinal and transverse relaxation rate, respectively. At low temperatures we have $\Gamma_1 \approx \Gamma_{1\downarrow}$. Assuming that pure dephasing $\Gamma_\varphi$ is small, we have

$$\Gamma_2 = \frac{\Gamma_1}{2} + \Gamma_\varphi \approx \frac{\Gamma_1}{2}. \tag{4.71}$$

Therefore, we obtain

$$\overline{\mathcal{E}}(t_g) = 1 - \frac{1}{6}(3 + \mathrm{e}^{-\Gamma_1 t_g} + 2\mathrm{e}^{-\Gamma_1 t_g/2}). \tag{4.72}$$

For large mean photon numbers $\overline{n}$, we may Taylor expand to

$$\begin{aligned}\overline{\mathcal{E}}(t_g) &\approx 1 - \frac{1}{6}\Big[3 + (1 - \Gamma_1 t_g + \ldots) + 2(1 - \Gamma_1 t_g/2 + \ldots)\Big] \\ &= \frac{1}{3}\Gamma_1 t_g \\ &= \frac{\pi^2}{6}\frac{1}{\overline{n}}.\end{aligned} \tag{4.73}$$

Hence, we conclude that the average infidelity is inversely proportional to the mean photon number, $\overline{n} \gg 1$. The same scaling was also observed in simulations of the subharmonic drive [12]. The average infidelity of the resonant drive was analytically calculated in [35] using the Jaynes-Cummings model with single-photon transitions. For large mean photon number $\overline{n}$ the power law of average infidelity was also proportional to $1/\overline{n}$. Our results therefore suggest that subharmonic driving does not offer an improvement in the scaling of infidelity compared to resonant driving.

# 5. Conclusions

This thesis provides a theoretical description of the decoherence of the transmon qubit under a novel control technique known as subharmonic driving. We begin with a comprehensive introduction to superconducting qubits and quantum driving, followed by fundamental concepts of non-equilibrium systems and decoherence, along with a mathematical framework for solving Langevin equations using harmonic analysis. The concept of subharmonic driving is introduced, and the subharmonic transmon Hamiltonian is derived in detail.

As a contribution to the literature, we then examine the case of a noisy subharmonic drive, calculating the decay rate caused by voltage fluctuations in the transmission line. To evaluate the correlation functions of the qubit response to the noisy drive, we apply the harmonic analysis methods previously established. The decay rate and pure dephasing rate are computed, and the average infidelity of a single quantum gate is determined as a function of the mean photon number.

The average infidelity is found to scale inversely with the mean photon number in the infinite photon limit, mirroring the scaling observed for resonant driving. This result is consistent with prior simulation experiments reported in [12].

Although subharmonic driving does not improve the scaling of infidelity, we discovered an unexpected result:: vacuum noise at an angular frequency of $5\omega_q/3$ contributes to the decay rate through a multiphoton process. The validity of this finding can be further tested through experimental and numerical research in the future.

In this thesis, we employ a semiclassical model where the qubit is treated as a quantum-mechanical system, while the driving field is modeled as classical. This approach leads to a correlation function represented by a non-convergent integral with a second-order pole in the frequency domain. Since the noise is semiclassical, the Hamiltonian lacks a dissipation term and functions solely as a drive on the qubit. Consequently, the qubit's response mimics that of an undamped harmonic oscillator, resulting in a second-order pole at resonance.

To circumvent this singularity, we assume that the power spectral density of the vacuum noise at the qubit frequency is zero, a condition that could be enforced using a band-stop filter. However, the existence of this pole indicates that the model may be incomplete. For a more comprehensive investigation of noisy subharmonic driving, future studies could possibly consider a fully quantum model with a bosonic bath.

# Bibliography


[1] A. Bayerstadler, G. Becquin, J. Binder, T. Botter, H. Ehm, T. Ehmer, M. Erdmann, N. Gaus, P. Harbach, M. Hess, and et al. Industry quantum computing applications. *EPJ Quantum Technology*, 8(1), Nov 2021.

[2] Lov K. Grover. A fast quantum mechanical algorithm for database search. In *Proceedings of the Twenty-Eighth Annual ACM Symposium on Theory of Computing*, page 212–219. Association for Computing Machinery, 1996.

[3] P.W. Shor. Algorithms for quantum computation: discrete logarithms and factoring. In *Proceedings 35th Annual Symposium on Foundations of Computer Science*, pages 124–134, 1994.

[4] I. Buluta, S. Ashhab, and F. Nori. Natural and artificial atoms for quantum computation. *Reports on Progress in Physics*, 74(10), 2011.

[5] M. Kjaergaard, M. E. Schwartz, J. Braumüller, P. Krantz, J. Wang, S. Gustavsson, and W. D. Oliver. Superconducting Qubits: Current State of Play. *Annual Review of Condensed Matter Physics*, 11(Volume 11, 2020), 2020.

[6] D. P. DiVincenzo. The physical implementation of quantum computation. *Fortschritte der Physik*, 48(9–11), 2000.

[7] A. Somoroff, Q. Ficheux, Raymond A. Mencia, H. Xiong, R. Kuzmin, and V. E. Manucharyan. Millisecond Coherence in a Superconducting Qubit. *Physical Review Letters*, 130, 2023.

[8] A. A. Clerk, M. H. Devoret, S. M. Girvin, Florian Marquardt, and R. J. Schoelkopf. Introduction to quantum noise, measurement, and amplification. *Reviews of Modern Physics*, 82, 2010.

[9] X. Mingkang, Z. Chao, L. Chenxu, P. Param, C. Xi, L. Pinlei, M. Boris, M. Maria, G. David, P. David, and H. Michael. Fast superconducting qubit control with subharmonic drives, 2023.

[10] J. Koch, T. M. Yu, J. Gambetta, A. A. Houck, D. I. Schuster, J. Majer, A. Blais, M. H. Devoret, S. M. Girvin, and R. J. Schoelkopf. Charge-insensitive qubit design derived from the Cooper pair box. *Physical Review A*, 76, 2007.

[11] U. Vool and M. Devoret. Introduction to quantum electromagnetic circuits. *International Journal of Circuit Theory and Applications*, 45(7), 2017.

[12] F. H. M. Ihamuotila. Simulations of Superconducting Qubits Under a Subharmonic Drive. Master's thesis, Aalto University, 2023. Available at https://aaltodoc.aalto.fi/items/ffe34772-831c-4d15-9744-795c8128accb.

[13] A. Blais, A. L. Grimsmo, S. M. Girvin, and A. Wallraff. Circuit quantum electrodynamics. *Reviews of Modern Physics*, 93, 2021.

[14] P. Krantz, M. Kjaergaard, F. Yan, T. P. Orlando, S. Gustavsson, and W. D. Oliver. A quantum engineer's guide to superconducting qubits. *Applied Physics Reviews*, 6(2), 2019.

[15] J. J. Sakurai and J. Napolitano. *Modern Quantum Mechanics*. Cambridge University Press, 3 edition, 2020.

[16] B.D. Josephson. Possible new effects in superconductive tunnelling. *Physics Letters*, 1(7), 1962.

[17] M. Tinkham. *Introduction to superconductivity*. McGraw-Hill, New York, 1996.

[18] F. London. *Superfluids*, volume 1. Dover, New York, 1960.

[19] V. Bouchiat, D. Vion, P. Joyez, D. Esteve, and M. H. Devoret. Quantum coherence with a single Cooper pair. *Physica Scripta*, 1998(T76), 1998.

[20] R. C. Jaklevic, J. Lambe, A. H. Silver, and J. E. Mercereau. Quantum interference effects in Josephson tunneling. *Physical Review Letters*, 12, 1964.

[21] E.T. Jaynes and F.W. Cummings. Comparison of quantum and semiclassical radiation theories with application to the beam maser. *Proceedings of the IEEE*, 51, 1963.

[22] C. Gerry and P. Knight. *Introductory Quantum Optics*. Cambridge University Press, 2004.

[23] N. Pottier. *Nonequilibrium Statistical Physics: Linear Irreversible Processes*. Oxford University Press, 2019.

[24] Hashitsume N. Kubo R., Toda M. *Statistical Physics II: Nonequilibrium Statistical Mechanics*. Springer Berlin, Heidelberg, 1991.

[25] N. Borghini. Topics in nonequilibrium physics. 2012.

[26] H. Nyquist. Thermal agitation of electric charge in conductors. *Physical Review*, 32, 1928.

[27] A.O Caldeira and A.J Leggett. Quantum tunnelling in a dissipative system. *Annals of Physics*, 149(2), 1983.

[28] J. M. Martinis, S. Nam, J. Aumentado, K. M. Lang, and C. Urbina. Decoherence of a superconducting qubit due to bias noise. *Physical Review B*, 67, 2003.

[29] A.G. Redfield. The theory of relaxation processes. volume 1 of *Advances in Magnetic and Optical Resonance*, pages 1–32. Academic Press, 1965.

[30] L. H. Pedersen, N. M. Møller, and K. Mølmer. Fidelity of quantum operations. *Physics Letters A*, 367(1–2), 2007.

[31] F. Bao, H. Deng, D. Ding, Ran Gao, Xun Gao, Cupjin Huang, X. Jiang, H. Ku, Z. Li, X. Ma, X. Ni, J. Qin, Z. Song, H. Sun, C. Tang, T. Wang, F. Wu, T. Xia, W. Yu, F. Zhang, G. Zhang, X. Zhang, J. Zhou, X. Zhu, Y. Shi, J. Chen, H. Zhao, and C. Deng. Fluxonium: An alternative qubit platform for high-fidelity operations. *Physical Review Letters*, 129(1), 2022.

[32] Aashish Sah, Suman Kundu, Heikki Suominen, Qiming Chen, and Mikko Möttönen. Decay-protected superconducting qubit with fast control enabled by integrated on-chip filters. *Communications Physics*, 7(1), 2024.

[33] R. J. Schoelkopf, A. A. Clerk, S. M. Girvin, K. W. Lehnert, and M. H. Devoret. *Qubits as Spectrometers of Quantum Noise*. Springer Netherlands, 2003.

[34] C. Yan, J. Hassel, V. Vesterinen, J. Zhang, J. Ikonen, L. Grönberg, J. Goetz, and M. Möttönen. A low-noise on-chip coherent microwave source. *Nature Electronics*, 4, 2021.

[35] J. Ikonen. Optimal Quantum Driving for Single-Qubit Gates. Master's thesis, University of Helsinki, 2015. Available at https://helda.helsinki.fi/server/api/core/bitstreams/43ec61b7-5b88-4334-b29b-28579c984f63/content.

# A. Supplementary calculations

## A.1 The displacement transformation

Here, we show that by applying the displacement transformation to the driven transmon Hamiltonian in Eq. (4.2), we obtain

$$\hat{H}^D/\hbar = \hat{D}(t)\hat{H}\hat{D}(t)^\dagger/\hbar + i\dot{\hat{D}}(t)\hat{D}(t)^\dagger \tag{A.1}$$

$$= \omega_p \hat{q}^\dagger \hat{q} + \frac{\alpha}{12}\left(\hat{q}^\dagger + \hat{q} - z^*(t) - z(t)\right)^4, \tag{A.2}$$

when $z(t)$ is as defined in (4.5). To begin we abbreviate $z \coloneqq z(t)$ and $\hat{D}(t) \coloneqq \hat{D}$. The main mathematical tool we use is the Baker-Campbell-Hausdorff formula

$$\mathrm{e}^{\hat{A}}\mathrm{e}^{\hat{B}} = \mathrm{e}^{\hat{A}+\hat{B}+\frac{1}{2}[\hat{A},\,B]+\frac{1}{12}[\hat{A},\,[\hat{A},\,\hat{B}]]+\ldots}, \tag{A.3}$$

and the Hadamard's lemma that follows from it:

$$\mathrm{e}^{A}\hat{B}\mathrm{e}^{-\hat{A}} = \hat{B} + [\hat{A},\,\hat{B}] + \frac{1}{2!}[\hat{A},\,[\hat{A},\,\hat{B}]] + \frac{1}{3!}[\hat{A},\,[\hat{A},\,[\hat{A},\,\hat{B}]]] \tag{A.4}$$

$$= \sum_{n=0}^{\infty} \frac{1}{n!}[\hat{A}, \ldots [\hat{A},\,[\hat{A},\,\hat{B}]]\ldots]. \tag{A.5}$$

Combining (A.4) with the commutation relation of the ladder operators gives the following identities

$$\hat{D}\hat{q}\hat{D}^\dagger = \hat{q} - z \tag{A.6}$$

$$\hat{D}\hat{q}^\dagger\hat{D}^\dagger = \hat{q}^\dagger - z^* \tag{A.7}$$

$$\hat{D}\hat{q}^\dagger\hat{q}\hat{D}^\dagger = \hat{D}\hat{q}^\dagger\hat{D}^\dagger\hat{D}\hat{q}\hat{D}^\dagger = \left(\hat{q}^\dagger - z^*\right)(\hat{q} - z), \tag{A.8}$$

where in the last line we used the unitarity of the displacement operator. Now, the first term in (A.1) becomes

$$\hat{D}\hat{H}\hat{D}^\dagger/\hbar = \omega_p \hat{D}\hat{q}^\dagger\hat{q}\hat{D}^\dagger + \frac{\alpha}{12}\hat{D}\left(\hat{q}^\dagger + \hat{q}\right)^4 \hat{D}^\dagger + \Omega(t)\hat{D}(\hat{q}^\dagger + \hat{q})\hat{D}^\dagger \tag{A.9}$$

$$= \omega_p \left(\hat{q}^\dagger - z^*\right)(\hat{q} - z) + \frac{\alpha}{12}\left(\hat{D}\left(\hat{q}^\dagger + \hat{q}\right)\hat{D}^\dagger\right)^4 + \Omega(t)(\hat{q}^\dagger + \hat{q} - z^* - z) \tag{A.10}$$

$$= \omega_p \left(\hat{q}^\dagger\hat{q} - z\hat{q}^\dagger - z^*\hat{q} + |z|^2\right) + \frac{\alpha}{12}\left(\hat{q}^\dagger + \hat{q} - z^* - z\right)^4 + \Omega(t)(\hat{q}^\dagger + \hat{q} - z^* - z). \tag{A.11}$$

Calculating the time derivative in (A.1) is not straightforward as the exponentiated operator does not commute with itself at different times. To circumvent this issue, we use (A.3) to obtain

$$\mathrm{e}^{z\hat{q}^\dagger - z^*\hat{q}} = \mathrm{e}^{z\hat{q}^\dagger}\mathrm{e}^{-z^*\hat{q}}\mathrm{e}^{-\frac{1}{2}[z\hat{q}^\dagger, -z^*\hat{q}]} \tag{A.12}$$

$$= \mathrm{e}^{z\hat{q}^\dagger}\mathrm{e}^{-z^*\hat{q}}\mathrm{e}^{-|z|^2/2} \tag{A.13}$$

The second term may now be evaluated using the ordinary chain-rule

$$i\dot{\hat{D}}\hat{D}^\dagger = i\frac{\partial}{\partial t}\left(\mathrm{e}^{z\hat{q}^\dagger - z^*\hat{q}}\right)\hat{D}^\dagger \tag{A.14}$$

$$= i\frac{\partial}{\partial t}\left(\mathrm{e}^{z\hat{q}^\dagger}\mathrm{e}^{-z^*\hat{q}}\mathrm{e}^{-|z|^2/2}\right)\hat{D}^\dagger \tag{A.15}$$

$$= i\left(\dot{z}\hat{q}^\dagger\mathrm{e}^{z\hat{q}^\dagger}\mathrm{e}^{-z^*\hat{q}}\mathrm{e}^{-|z|^2/2} - \dot{z}^*\mathrm{e}^{z\hat{q}^\dagger}\hat{q}\mathrm{e}^{-z^*\hat{q}}\mathrm{e}^{-|z|^2/2} - \mathrm{Re}(\dot{z}z^*)\mathrm{e}^{z\hat{q}^\dagger}\mathrm{e}^{-z^*\hat{q}}\mathrm{e}^{-|z|^2/2}\right)\hat{D}^\dagger \tag{A.16}$$

$$= i\left(\dot{z}\hat{q}^\dagger\hat{D} - \dot{z}^*(\hat{q} - z)\mathrm{e}^{z\hat{q}^\dagger}\mathrm{e}^{-z^*\hat{q}}\mathrm{e}^{|z|^2/2} - \mathrm{Re}(\dot{z}z^*)\hat{D}\right)\hat{D}^\dagger \tag{A.17}$$

$$= i\left(\dot{z}\hat{q}^\dagger - \dot{z}^*\hat{q} - \mathrm{Im}(\dot{z}z^*)\right). \tag{A.18}$$

In the fourth equality, to isolate $\hat{q}$ from the middle, we applied the formula

$$[\hat{q}, f(\hat{q}^\dagger)] = \frac{\partial}{\partial\hat{q}^\dagger}f(\hat{q}^\dagger), \tag{A.19}$$

where $f$ is any function with a power series representation. Neglecting the constant terms, combining the results gives

$$\hat{H}^D/\hbar = \omega_p\left(\hat{q}^\dagger\hat{q} - z\hat{q}^\dagger - z^*\hat{q}\right) + \frac{\alpha}{12}\left(\hat{q}^\dagger + \hat{q} - z^* - z\right)^4 + i\left(\dot{z}\hat{q}^\dagger - \dot{z}^*\hat{q}\right) + \Omega(t)(\hat{q}^\dagger + \hat{q}) \tag{A.20}$$

$$= \omega_p\hat{q}^\dagger\hat{q} + \frac{\alpha}{12}\left(\hat{q}^\dagger + \hat{q} - z^* - z\right)^4 + (\Omega(t) + i\dot{z} - \omega_p z)\hat{q}^\dagger + (\Omega(t) - i\dot{z}^* - \omega_p z^*)\hat{q} \tag{A.21}$$

$$\tag{A.22}$$

The unwanted terms vanish, if we require

$$\Omega(t) + i\dot{z} - \omega_p z = 0 \tag{A.23}$$

$$\Omega(t) - i\dot{z}^* - \omega_p z^* = 0. \tag{A.24}$$

By noting that the second equation is the adjoint of the first, we arrive the wanted result in Eq. (4.4).

## A.2 The rotating frame

Here, we evaluate the unitary transformation

$$\hat{H}_{\mathrm{R}}/\hbar = \hat{U}_{\mathrm{R}}\hat{H}_{\mathrm{D}}\hat{U}_{\mathrm{R}}^{\dagger}/\hbar + i\dot{\hat{U}}_{\mathrm{R}}\hat{U}_{\mathrm{R}}^{\dagger}. \tag{A.25}$$

Using (A.4) we get

$$\hat{R}\hat{q}^{\dagger}\hat{R}^{\dagger} = \mathrm{e}^{\mathrm{i}3\omega_d t\hat{q}^{\dagger}\hat{q}}\hat{q}^{\dagger}\mathrm{e}^{-\mathrm{i}3\omega_d t\hat{q}^{\dagger}\hat{q}} \tag{A.26}$$

$$= \sum_{n=0}^{\infty}\frac{(i3\omega_d t)^n}{n!}[\hat{q}^{\dagger}\hat{q}, \ldots [\hat{q}^{\dagger}\hat{q},\, [\hat{q}^{\dagger}\hat{q},\, \hat{q}^{\dagger}]]\ldots] \tag{A.27}$$

$$= \sum_{n=0}^{\infty}\frac{(i3\omega_d t)^n}{n!}\hat{q}^{\dagger} = \mathrm{e}^{\mathrm{i}3\omega_d t}\hat{q}^{\dagger}, \tag{A.28}$$

where we used the commutator $[\hat{q}^{\dagger}\hat{q},\, \hat{q}^{\dagger}] = \hat{q}^{\dagger}$. The adjoint of above equation gives

$$\hat{R}\hat{q}\hat{R}^{\dagger} = \mathrm{e}^{-\mathrm{i}3\omega_d t}\hat{q}. \tag{A.29}$$

This time the time derivative is straightforward to compute

$$i\dot{\hat{R}}\hat{R} = i(\frac{\partial}{\partial t}\mathrm{e}^{\mathrm{i}3\omega_d t\hat{q}^{\dagger}\hat{q}})\hat{R} = -3\omega_d\hat{q}^{\dagger}\hat{q}. \tag{A.30}$$

With these identities, (A.25) becomes

$$\hat{H}_{\mathrm{R}}/\hbar = \omega_p\hat{q}^{\dagger}\hat{q} + \frac{\alpha}{12}\hat{R}\left(\hat{q}^{\dagger} + \hat{q} + \eta\mathrm{e}^{-\mathrm{i}\omega_d t} + \eta^*\mathrm{e}^{\mathrm{i}\omega_d t}\right)^4\hat{R}^{\dagger} - 3\omega_d\hat{q}^{\dagger}\hat{q} \tag{A.31}$$

$$= (\omega_p - 3\omega_d)\hat{q}^{\dagger}\hat{q} + \frac{\alpha}{12}\left(\hat{q}^{\dagger}\mathrm{e}^{\mathrm{i}3\omega_d t} + \hat{q}\mathrm{e}^{-\mathrm{i}3\omega_d t} + \eta\mathrm{e}^{-\mathrm{i}\omega_d t} + \eta^*\mathrm{e}^{\mathrm{i}\omega_d t}\right)^4. \tag{A.32}$$

## A.3 The rotating wave approximation

Under the rotating wave approximation, individual terms that survive satisfy the condition $m - n - 3i + 3j = 0$. These terms can be categorized into four groups:

$$\text{A)} \quad i = j = 2 \text{ and } m = n = 0, \tag{A.33}$$
$$\text{B)} \quad i = j = 1 \text{ and } m = n = 1, \tag{A.34}$$
$$\text{C)} \quad i = 1,\ j = 0,\ m = 3 \text{ and } n = 0, \tag{A.35}$$
$$\text{D)} \quad i = 0,\ j = 1,\ m = 0 \text{ and } n = 3. \tag{A.36}$$
$$\tag{A.37}$$

Group A consists of the six terms

$$\hat{q}^\dagger\hat{q}^\dagger\hat{q}\hat{q} \tag{A.38}$$
$$\hat{q}^\dagger\hat{q}\hat{q}^\dagger\hat{q} = \hat{q}^\dagger\hat{q}^\dagger\hat{q}\hat{q} + \hat{q}^\dagger\hat{q} \tag{A.39}$$
$$\hat{q}\hat{q}\hat{q}^\dagger\hat{q}^\dagger = \hat{q}^\dagger\hat{q}^\dagger\hat{q}\hat{q} + 4\hat{q}^\dagger\hat{q} + 2 \tag{A.40}$$
$$\hat{q}\hat{q}^\dagger\hat{q}\hat{q}^\dagger = \hat{q}^\dagger\hat{q}^\dagger\hat{q}\hat{q} + 3\hat{q}^\dagger\hat{q} + 1 \tag{A.41}$$
$$\hat{q}^\dagger\hat{q}\hat{q}\hat{q}^\dagger = \hat{q}^\dagger\hat{q}^\dagger\hat{q}\hat{q} + 2\hat{q}^\dagger\hat{q} \tag{A.42}$$
$$\hat{q}\hat{q}^\dagger\hat{q}^\dagger\hat{q} = \hat{q}^\dagger\hat{q}^\dagger\hat{q}\hat{q} + 2\hat{q}^\dagger\hat{q}, \tag{A.43}$$

where on the right-hand side, terms are arranged in normal order. Group B comprises 24 terms:

$$12|\eta|^2(\hat{q}^\dagger\hat{q} + \hat{q}\hat{q}^\dagger) = 24|\eta|^2\hat{q}^\dagger\hat{q} + 12|\eta|^2. \tag{A.44}$$

Groups C and D both consist of four terms, the sum of which gives

$$4(\eta^3\hat{q}^\dagger + \eta^{*3}\hat{q}). \tag{A.45}$$

Thus the total sum of the surviving terms is

$$6\hat{q}^\dagger\hat{q}^\dagger\hat{q}\hat{q} + (24|\eta|^2 + 12)\hat{q}^\dagger\hat{q} + 4(\eta^3\hat{q}^\dagger + \eta^{*3}\hat{q}), \tag{A.46}$$

where we again omitted the constant terms. The subharmonic Hamiltonian then becomes

$$\hat{H}_{\mathrm{R}}^{\mathrm{RWA}}/\hbar \coloneqq (\omega_p - 3\omega_d)\hat{q}^\dagger\hat{q} + \frac{\alpha}{12}\left(6\hat{q}^\dagger\hat{q}^\dagger\hat{q}\hat{q} + (24|\eta|^2 + 12)\hat{q}^\dagger\hat{q} + 4(\eta^3\hat{q}^\dagger + \eta^{*3}\hat{q})\right) \tag{A.47}$$

$$= (\omega_p - 3\omega_d + 2\alpha|\eta|^2 + \alpha)\hat{q}^\dagger\hat{q} + \frac{\alpha}{2}\hat{q}^\dagger\hat{q}^\dagger\hat{q}\hat{q} + \frac{\alpha}{3}(\eta^3\hat{q}^\dagger + \eta^{*3}\hat{q}) \tag{A.48}$$

$$= (2\alpha|\eta|^2 - 3\delta)\hat{q}^\dagger\hat{q} + \frac{\alpha}{2}\hat{q}^\dagger\hat{q}^\dagger\hat{q}\hat{q} + \frac{\alpha}{3}(\eta^3\hat{q}^\dagger + \eta^{*3}\hat{q}), \tag{A.49}$$

where in the last line we substituted $\omega_p = \omega_q - \alpha$ and $\omega_d = \omega_q/3 + \delta$.